11-1-2022

The programmed death-1 signaling axis modulates inflammation and LV structure/function in a stress-induced cardiomyopathy model

Tomohiro Hayashi

Sajal K Tiwary

Kory J Lavine

Sandeep Acharya

Michael Brent

See next page for additional authors

Authors

Tomohiro Hayashi, Sajal K Tiwary, Kory J Lavine, Sandeep Acharya, Michael Brent, Luigi Adamo, Attila Kovacs, and Douglas L Mann

JACC: BASIC TO TRANSLATIONAL SCIENCE
PUBLISHED BY ELSEVIER ON BEHALF OF THE AMERICAN COLLEGE OF CARDIOLOGY FOUNDATION.

VOL. 7, NO. 11, 2022

ORIGINAL RESEARCH - PRECLINICAL

The Programmed Death-1 Signaling Axis Modulates Inflammation and LV Structure/Function in a Stress-Induced Cardiomyopathy Model

Tomohiro Hayashi, MD, PhD,[a] Sajal K. Tiwary, MD,[a] Kory J. Lavine, MD, PhD,[a] Sandeep Acharya,[b] Michael Brent, PhD,[b,c] Luigi Adamo, MD, PhD,[d] Attila Kovacs, MD,[a] Douglas L. Mann, MD[a]

VISUAL ABSTRACT

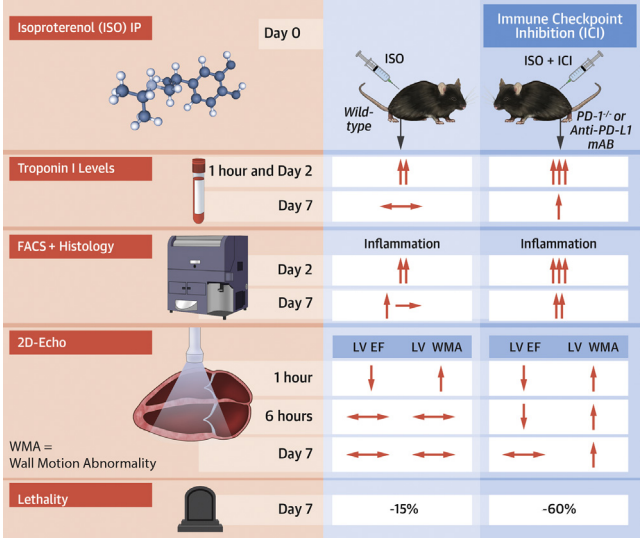

Hayashi T, et al. J Am Coll Cardiol Basic Trans Science. 2022;7(11):1120–1139.

HIGHLIGHTS

- A single intraperitoneal dose of ISO provokes an acute inflammatory response in the heart that is accompanied by reversible changes in LV structure and function.
- Single-cell RNA sequencing reveals that ISO injury elicits a transient increase in expression of multiple inhibitory immune checkpoints genes, including *Pdcd1* (PD-1) and *Cd274* (PD-L1), predominantly in the cardiac resident innate immune cells, including LYVE1^{-} macrophages and dendritic cells.
- Treatment with an anti-PD-L1 antibody results in increased myocardial inflammation after ISO injection, whereas ISO injection in PD-1$^{-/-}$ mice results in increased duration of the inflammatory response, prolonged LV dilation, and LV dysfunction relative to wild-type mice.
- In vitro stimulation of peritoneal derived inflammatory cells with necrotic cardiac myocytes increases the percentage of cells expressing PD-1 in macrophages and T cells in a TLR2/TLR4/NF-κB-dependent manner.

From the [a]Center for Cardiovascular Research, Cardiovascular Division, Department of Medicine, Washington University School of Medicine, St Louis, Missouri, USA; [b]Department of Computer Science, Washington University, St Louis, Missouri, USA; [c]Center for Genome Sciences and Systems Biology, Washington University School of Medicine, St Louis, Missouri, USA; and the [d]Division of Cardiology, Johns Hopkins University School of Medicine, Baltimore, Maryland, USA.

Peter Liu, MD, served as Guest Associate Editor for this paper. Michael Bristow, MD, PhD, served as Guest Editor-in-Chief for this paper.

ISSN 2452-302X https://doi.org/10.1016/j.jacbts.2022.05.006

SUMMARY

The role of immune checkpoints in the setting of tissue injury remains unknown. Using an experimental model of isoproterenol (ISO)-induced stress cardiomyopathy, we show that ISO-induced myocardial injury provokes tissue-autonomous up-regulation of the programmed death-1 (PD-1):programmed death ligand (PD-L) axis in cardiac resident innate immune cells and T cells. PD-1 signaling was responsible for modulating the acute inflammatory response, as well as normalization of impaired left ventricular structure and function after ISO injection. Necrotic cardiac extracts were sufficient to increase the expression of PD-1 in macrophages and T cells in vitro. Viewed together these studies suggest that the PD-1:PD-L signaling axis regulates immune responses to cardiac tissue injury and is important for restoring myocardial homeostasis.
(J Am Coll Cardiol Basic Trans Science 2022;7:1120–1139) Published by Elsevier on behalf of the American College of Cardiology Foundation.

ABBREVIATIONS AND ACRONYMS

ICI = immune checkpoint inhibitor
ISO = isoproterenol
LV = left ventricle/ventricular
PD-1 = programmed death-1
PD-L1 = PD-ligand 1
PD-L2 = PD-ligand 2
TLR = Toll-like receptor

Myocardial injury resulting from invading pathogens or environmental stress (such as ischemia or hemodynamic overloading) leads to activation of the innate and adaptive immune systems to engender tissue repair and restore myocardial homeostasis. This short-term adaptation to stress has been termed "physiological inflammation."[1] The resolution of physiological inflammation has traditionally been viewed as a highly coordinated active process that involves the down-regulation of pro-inflammatory cytokine responses, termination of chemokine signaling, clearance of apoptotic neutrophils and cardiac myocytes, recruitment of regulatory T cells, and functional repolarization of resident macrophage populations (reviewed by Frangogiannis[2]). Additionally, an accumulating body of evidence suggests that the resolution of inflammation requires up-regulation of pro-resolving molecular pathways that are initiated shortly after the onset of the inflammation, including the up-regulation of a suite of anti-inflammatory molecules (eg, interleukin-10 and members of the transforming growth factor family), as well as up-regulation of pro-resolving lipid mediators, such as lipoxins, resolvins, and protectins that suppress pro-inflammatory signaling.[2-4] If the inflammatory response becomes excessive and/or prolonged, it can lead to collateral tissue damage that results in adverse cardiac remodeling and progressive cardiac dysfunction.[5]

Immune checkpoints are phylogenetically conserved molecules[6] that act as gate keepers of the immune response by providing critically timed inhibitory and stimulatory signals to immune cells that determine the strength and duration of the immune response, thereby optimizing the immune response and preserving tissue integrity.[7] Our current understanding of the role of immune checkpoint pathways is largely derived from seminal research in the field of cancer immunotherapy. By studying how the immune system interfaces with solid and hematologic malignancies and understanding how cancer cells exploit the use of immune checkpoints to suppress immune responses and avoid immune detection, investigators have developed therapeutic antibodies (Abs) that block inhibitory immune checkpoint pathways, thereby restoring the ability of T cells to mount effective antitumor responses. The clinical observation that treatment with immune checkpoint inhibitors (ICIs) is associated with the loss of self-tolerance and the development of autoimmune phenomena that impact multiple organ systems, including the heart, highlights the critical role of immune checkpoints in terms of modulating immune responses. Indeed, programmed death-1 (PD-1) (CD279) deficient BALB/c mice spontaneously develop autoimmune dilated cardiomyopathy.[8,9] However, the broader teleological question of whether immune checkpoints maintain organ homeostasis by modulating the immune response to tissue injury has not been explored. Here, we use an experimental model of reversible stress-induced cardiomyopathy to investigate the role of immune checkpoints during acute injury and repair (ie, physiological inflammation). We show that transient myocardial tissue injury up-regulates the canonical PD-1 signaling axis not only in T cells, but also in

The authors attest they are in compliance with human studies committees and animal welfare regulations of the authors' institutions and Food and Drug Administration guidelines, including patient consent where appropriate. For more information, visit the Author Center.

Manuscript received March 8, 2022; revised manuscript received May 24, 2022, accepted May 24, 2022.

resident innate immune cells. Remarkably, disrupting the PD-1/PD-ligand 1 (PD-L1) (B7-H1, CD274)/PD-ligand 2 (PD-L2) (B7-DC, CD273) signaling axis increases and prolongs the myocardial inflammatory response to tissue injury, leading to increased collateral tissue damage and delayed normalization of left ventricular (LV) structure and function. Viewed together, these studies highlight a previously unprecedented role for the PD-1:PD-L signaling axis in regulating intrinsic physiological inflammatory responses and restoring organ homeostasis after tissue injury.

METHODS

MICE. C57BL/6J (stock number 000664) and PD-1$^{-/-}$ (C57BL/6J; B6.Cg-*Pdcd1*$^{tm1.1Shr}$/J; stock number 028276) mice were purchased from The Jackson Laboratory. The mouse colonies were maintained in a pathogen-free environment at the Washington University School of Medicine and were fed pellet food and water at libitum. Because stress-induced cardiomyopathy predominantly occurs in women,[10] we focused the majority of our studies on the response of 10-week-old female C57BL/6J mice and 10-week-old female PD-1$^{-/-}$ deficient mice. To determine whether there were sex-related differences, we repeated core experiments with 10-week-old male C57BL/6J mice.

STUDY APPROVAL. All experimental procedures were performed in accordance with approved animal protocols from the Institutional Animal Care and Use Committee at Washington University School of Medicine. These investigations conform to the National Institutes of Health Guide for the Care and Use of Laboratory Animals.

INDUCTION OF STRESS-INDUCED CARDIOMYOPATHY. Mice were injected intraperitoneally (IP) with a single dose of 300 mg/kg of isoproterenol hydrochloride (ISO) (Sigma-Aldrich). ISO was dissolved in endotoxin-free phosphate buffer saline (PBS) (Millipore; 0.05 mg/μl) and prepared on ice for immediate use. Control mice were injected IP with PBS at an equivalent volume. The heart, blood, and spleen were harvested at baseline (before ISO injection); at 1 hour following ISO or PBS injection; and at 1 (24 hours), 2, 3, 4, and 7 days following ISO or PBS injection.

PD-1–, PD-L1–, AND PD-L2–BLOCKING ANTIBODIES. To explore the role of PD-1 and PD-1 ligands in ISO-induced stress-induced cardiomyopathy, anti-PD-1, anti-PD-L1, anti-PD-L2, or isotype control Abs were administered IP at a dose of 300 μg per mouse.[11,12] The following Abs (Bio X Cell) were employed: rat anti-PD-1 (clone RMP1-14); rat anti-PD-L1 (clone 10F.9G2); rat IgG2b (clone LTF-2), isotype control for anti-PD-L1; rat anti-PD-L2 (clone TY25); and rat IgG2a (clone 2A3), isotype control for anti-PD-1 and anti-PD-L2.[11] All Abs were diluted in InVivoPure dilution buffers (Bio X Cell) to a concentration of 1 mg/mL just prior to use, according to the manufacturer's instructions. Mice received Ab injections 2 days before, and 1 and 4 days after ISO administration.

CYTOTOXIC T LYMPHOCYTE-ASSOCIATED ANTIGEN-4 IG. To prevent T cell activation in ISO-induced stress-induced cardiomyopathy, recombinant cytotoxic T lymphocyte-associated antigen-4 (CTLA4) Ig or recombinant human isotype control IgG1 Ab were administered IP, at a dose of 200 μg per mouse.[13,14] The Abs were obtained from Bio X Cell and diluted in InVivoPure dilution buffers (Bio X Cell) to a concentration of 1 mg/mL just prior to use, according to the manufacturer's instructions. Mice received injections 2 days before and 1 and 4 days after ISO administration.

SERUM TROPONIN I LEVELS. Serum troponin I was measured using the ARCHITECT i2000 analyzer (Abbot Laboratories). Blood was collected by mandibular bleeding in BD Microtainer tubes at the time of terminal sacrifice. The serum was diluted 1:4 in PBS (80 μL serum + 240 μL PBS).

GRAVIMETRIC AND HISTOLOGICAL ANALYSIS. Mice were sacrificed at baseline; at 1 hour after ISO injection; and at 1, 2, 3, and 7 days after ISO injection, and the hearts were removed and weighed to determine the heart weight/tibia length ratio. Hearts were processed, paraffin-embedded, and stained with hematoxylin and eosin and Masson's trichrome, as described previously. Myocardial inflammation was assessed in sections stained with hematoxylin and eosin. The degree of myocardial inflammation was scored semiquantitatively in the following manner using an inflammatory score index: 0 = no infiltrate; 1+ = infiltrates involving <25% of the ventricular myocardium; 2+ = infiltrates involving 25%-50% of the myocardium; 3+ = infiltrates involving 50%-75% of the myocardium; and 4+ = infiltrates involving 75%-100% of the myocardium, as described.[15]

ECHOCARDIOGRAPHIC STUDIES. Image acquisition. Ultrasound examination of the heart was performed using the Vevo 2100 ultrasound system (VisualSonics) equipped with a 30-MHz linear array transducer as described.[16,17] Avertin (2,2,2-tribromoethanol, 2.5% solution, 0.005 mL/g body weight IP) was used for sedation for all imaging studies.

Imaging protocol. Mice were imaged by echocardiography at baseline and at 1 hour, 6 hours, and 7 days

after ISO injection to evaluate LV regional and global structure and function, as described.[17] Global LV size and function was evaluated by subjecting the parasternal long-axis movie loops of the LV to the speckle-tracking based strain analysis software implemented in the Vevo 2100 system (VevoStrain).[17]

Assessment of LV regional wall motion. LV regional wall motion was assessed from the base to apex of the LV. Briefly, 7 2-dimensional (2D) short-axis movie loops of the LV were acquired from the base to apex by manually advancing the transducer in 1-mm increments. Each of the 7 short-axis images was divided into 12 radial segments. LV wall motion within each segment was assessed visually and determined as normal (score = 1), hypokinetic (score = 2), or akinetic (score = 3), adopted from guidelines by the American Society of Echocardiography and validated in mouse studies as described.[18,19] Ultrasound studies were performed by an experienced operator blinded to the experimental protocol. The results were displayed as a bull's eye plot configured to display 7 myocardial cross sections so that the inner ring represents the apex of the LV, the middle ring represents the segments of the mid-LV, and the outer ring represents the basal segments of the LV, with each cross section subdivided into 12 radial sections (total of 84 segments). Segmental wall motion score index (SWMSI) was calculated as the ratio of the sum of the wall motion scores over all of the segments scored (values >1 indicate abnormal segmental wall motion).

FLOW CYTOMETRY. Isolation of leukocytes from the heart. Mice were sacrificed in a CO_2 chamber. Hearts were perfused and finely minced, as described.[20] Hearts were digested with collagenase type I (Sigma-Aldrich; 450 U/mL), DNAse I type II (Sigma-Aldrich; 60 U/mL), and hyaluronidase type I-S (Sigma-Aldrich; 60 U/mL) in a final volume of 3 mL of Hank's balanced salt solution (HBSS) for 45 minutes at 37 °C with agitation. The digested sample was supplemented with 6 mL of 2% fetal bovine serum (FBS) plus 0.2% bovine serum albumin in HBSS to block the enzymatic activity, and then filtered using 40-μm cell strainers and pelleted by centrifugation (350 *g* for 7 minutes at 4 °C). Red blood cells were lysed using ACK lysing buffer (Gibco) for 15 minutes on ice, and the remaining cells were resuspended in 200 μL of FACS buffer (PBS with 2% FBS and 2 mmol/L EDTA), stained with conjugated antibodies (see Supplemental Table S1) for 30 minutes at 4 °C, and washed with FACS buffer before analysis. Data were acquired using Becton Dickinson analyzers (BD X20 or LSRFortessa) at the Washington University Department of Pathology Flow Cytometry and Sorting Core facility. Compensation controls were generated using UltraComp eBeads (Invitrogen) and verified on single-color control samples obtained by staining primary splenocytes. The gating strategies are summarized in Supplemental Figure S1. Cell cytometric data were analyzed by FlowJo software (Tree Star).

Isolation of leukocytes from the blood and spleen. The lysis of red blood cells, staining, and acquisition were as described in the previous text. Blood obtained by mandibular bleeding was collected into tubes containing EDTA (Sarstedt). Data are shown as the number of cells/20 μL of blood. Spleens were removed and finely minced using 40-μm filters in HBSS with 2% FBS and 0.2% bovine serum albumin. Data are shown as the percentage of $CD45^+$ cells isolated from the spleen (n = 400,000 cells). The gating strategies are summarized in Supplemental Figures S2 (blood) and S3 (spleen).

CELL SORTING AND SINGLE-CELL TRANSCRIPTIONAL PROFILING. We used the Chromium Single Cell 3' v3 or 5' Library Kit and Chromium Instrument (both from 10x Genomics) to perform single-cell transcriptional analyses.

Myocardial $CD45^+$ leukocytes. We performed 5' sequencing and performed transcriptional profiling of cardiac $CD45^+$ leukocytes isolated from the whole hearts of wild-type (WT) mice (10 weeks of age) at 3 time points: baseline and days 2 and 7 post-ISO injection. Myocardial cells were isolated as described in the "Flow cytometry" section. After digestion and removing red blood cells, myocardial cells isolated from 3 mice at each time point were pooled together in 1 tube, respectively (3 tubes containing 3 hearts/tube). The remaining cells were resuspended in 200 μL of FACS buffer containing 1 μL of TruStain FcX Plus (Fc blocker; BioLegend). A total of 1 μL of Zombie Aqua Fixable Viability Kit (BioLegend) and 1 μL of CD45/PerCP-Cy5.5 Ab were added to each tube. They were also labelled with Hashtag-C Abs. The sample at the baseline was labelled with Hashtag-C #1, day 2 with Hashtag-C #2, and day 7 with Hashtag-C #3 (see Supplemental Table S2 for details). Cells were incubated for 30 minutes at 4 °C, protected from light, and then washed twice with FACS buffer. Approximately 20,000 $CD45^+Aqua^-$ cells (doublets excluded) were sorted from the tube of each time point using an FACS Aria-II Cell Sorter. Sorted $CD45^+Aqua^-$ cells were collected in DMEM containing 5% FBS. All heart cells were mixed in 1 tube and centrifuged at 350 *g*, 4 °C for 10 minutes (acceleration 7 and brake 0). $CD45^+Aqua^-$ cells were resuspended in DMEM containing 5% FBS

(35 μL in total) and submitted to the McDonnell Genome Institute at Washington University for further analysis.[20,21]

SINGLE-CELL RNA SEQUENCING AND MAPPING. The Seurat package in R (R Foundation for Statistical Computing) was used for all subsequent analyses.[22] Cells that expressed fewer than 500 genes or that were unlabeled or doublets per Hashtag Ab labeling were removed. For normalization, scaling, and variance stabilization of count data, the SCTransform package was used with concomitant regression of cells with high mitochondrial DNA counts.[23] Integration was performed instead of standard RNA processing and cluster identification because of concern for cells switching identity classes across time points. Cells were integrated using anchors identified across time points from the top 3,000 most variable genes and 29 dimensions from the anchor data set using the IntegrateData function of Seurat.[24] Cell clustering was performed on the integrated data set using principal-components analysis. The top 15 principal components were selected based on JackStraw and Elbow plots of the principal-components analysis. The FindClusters function was then used to perform k-nearest neighbor clustering with a resolution of 0.25 on the integrated assay. For cluster identification, the FindAllMarkers function was used to determine the top 20 differentially expressed markers by cluster that were expressed in at least 25% of cells and had a differential $\log_2$ fold change of at least 0.25. These markers were then passed to the "My Geneset" tool provided by the Immunological Genome Project for cell-type identification.[25] For differential gene expression analysis, a standard nonintegrated processing workflow was used, as previously described.[21] Briefly, cells with mitochondrial DNA content >7%, fewer than 200 unique feature counts, or >5,000 unique feature counts were removed. Data were then normalized using a scale factor of 10,000 and log transformed. The FindVariableFeatures function was used to select highly variable genes with mean >0.0125 or <3, and dispersion >0.5. The MAST algorithm in the Seurat FindMarkers function was used to determine differential gene expression between time points for individual clusters with a minimum cell expression percentage of 10%, a minimum $\log_2$ fold change of 0.25, and an adjusted *P* value of at least 0.05. Pseudobulk data set analysis was performed by summing normalized gene counts across all cells at each time point. Log_2 fold changes of each ratio of gene counts at a time point relative to counts at baseline were then determined for each gene.

CELL CULTURE. Peritoneal-derived inflammatory cells (PDICs) were isolated from 10-week-old WT mice 4 days after IP injection of 1 mL of thioglycolate medium (Millipore), as described.[26] PDICs were plated at 1.5×10^6 cells/mL in 12-well plates and cultured in DMEM with 10% FBS, 1 mmol/L sodium pyruvate, 100 U/mL penicillin/streptomycin, 2 mmol/L L-glutamine, 10 mmol/L HEPES, and 55 μmol/L 2-mercaptoethanol. Necrotic myocardial cell extracts (NCEs) were prepared from 10-week-old WT mouse hearts as described previously.[27] Cells were treated with 10 μg/mL NCEs, 200 ng/mL Toll-like receptor 2 (TLR2) agonist Pam3CSK4 (InvivoGen),[28] 100 ng/mL TLR4 agonist lipopolysaccharide (LPS) (LPS-EB Ultrapure, InvivoGen),[26] ISO (1, 10, or 100 μmol/L),[29] 4 μg/mL rat IgG2a (clone eBR2a, eBioscience), 4 μg/mL anti-mTLR2 Ab (clone C9A12, InvivoGen),[30] 10 μg/mL anti-mTLR4 Ab (clone MTS510, GeneTex),[27] and 1 μmol/L IMD-0354 (IKKβ/NF-κB inhibitor) (Tocris).[31] PDICs were cultured with Pam3CSK4, LPS, or NCEs for 72 hours. The cells were preincubated with IgG2a, anti-TLR2 ab, anti-TLR4 ab, or IMD-0354 for 30 minutes before stimulation with NCEs. For FACS analysis, both adherent and nonadherent cultured cells were collected. To collect the adherent fraction, cells were incubated for 30 minutes at 37 °C with Cellstripper (Corning). The adherent cells were mixed with the nonadherent cells, spun down at 250 *g* for 3 minutes at 4 °C, and resuspended in 200 μL of FACS buffer for further analysis by FACS. Dead cells were excluded using Zombie Aqua staining (BioLegend). Macrophages were gated as $CD45^+Aqua^-$ $CD64^+$, CD4 T cells: $CD45^+Aqua^-$ $CD4^+$, and CD8 T cells: $CD45^+Aqua^-$ $CD8^+$, respectively. Ab specifications, staining, acquisition, and data analysis are described in the "Flow Cytometry" section.

STATISTICAL ANALYSIS. All data are presented as mean ± SEM. The Shapiro-Wilk test was used to determine whether the data were normally distributed. The Kaplan-Meier survival curves were analyzed using the log-rank (Mantel-Cox) test. Statistical comparisons between 2 experimental groups were performed using the 2-tailed Student's *t-test*. One-way analysis of variance (ANOVA) with Dunnett's (multiple comparisons to a control) or Tukey's (all pairwise comparisons) correction for multiple post hoc comparisons were performed where appropriate. For 2-way ANOVA, a Sidak's correction was used for post hoc comparisons. To analyze the time-dependent changes in data, repeated measures ANOVA were used to adjust for within-group correlations. Otherwise, the data were analyzed using standard ANOVA for multiple comparisons. All data

FIGURE 1 Characterization of Stress Induced Cardiomyopathy Model

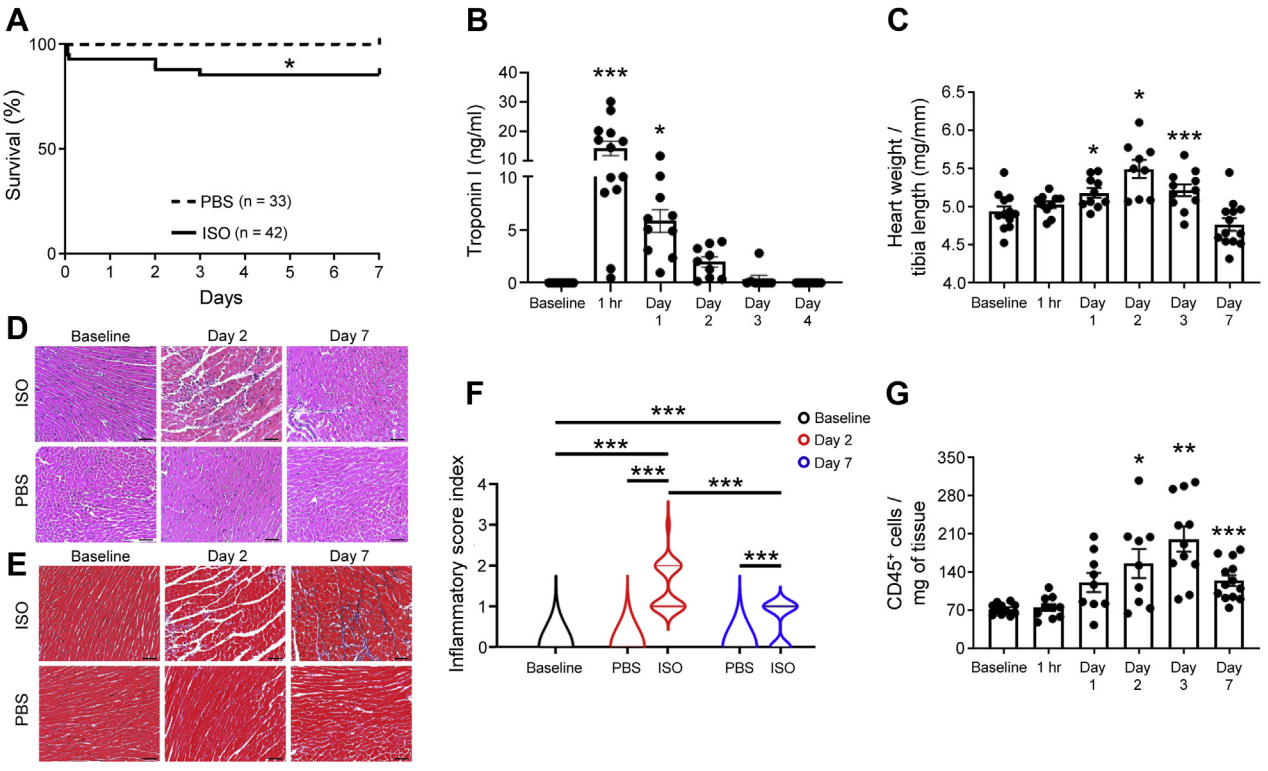

(A) Kaplan-Meier survival curves of isoproterenol (ISO)-injected (n = 42) and diluent injected (phosphate buffer saline [PBS]) control mice (n = 33). **(B)** Serum troponin I levels at baseline, 1 hour, and days 1-4 in ISO-treated mice (n = 7-12 mice/time). **(C)** Gravimetric analysis of hearts harvested from ISO-treated mice at baseline (n = 12), 1 hour, and days 1-3 and 7 (n = 9-13 hearts/time). **(D)** Representative photographs of hematoxylin and eosin–stained hearts at baseline and days 2 and 7 after ISO or diluent injection (scale bar = 50 μm). **(E)** Representative photographs of Masson's trichrome-stained hearts at baseline and days 2 and 7 after ISO or diluent injection (scale bar = 50 μm). **(F)** Inflammatory score index at baseline and days 2 and 7 after ISO or diluent injection (n = 24 fields obtained from 4 hearts/time). **(G)** Flow cytometry analysis of the number of $CD45^{+}$ cells/mg of heart tissue at baseline (n = 11 hearts), 1 hour, and days 1-3 and 7 (n = 9-13 hearts/time) after ISO injection. Data were analyzed by repeated measures 1-way analysis of variance with Dunnett's multiple comparisons relative to baseline **(B, C, and G)** or by repeated measures 2-way analysis of variance with Sidak's multiple comparisons **(F)**. *$P < 0.05$; **$P < 0.01$; ***$P < 0.001$.

were analyzed using GraphPad Prism version 8. A P value <0.05 was considered statistically significant.

RESULTS

CHARACTERIZATION OF MURINE MODEL OF STRESS-INDUCED CARDIOMYOPATHY. To select the optimal dose of ISO, dose titration studies were performed in WT C57BL/6J female mice (10 weeks of age) injected with a single dose of 100, 200, or 300 mg/kg (IP) of ISO. As shown in Supplemental Figure S4, the degree of inflammation was proportional to the degree of cardiac injury, as assessed by troponin I release. We found that 300 mg/kg (IP) of ISO produced the greatest injury with the greatest inflammatory response. Therefore, 300 mg/kg of ISO was used for all experiments in this study. Control WT C57BL/6J were injected IP with an equal volume of diluent (PBS). ISO-injected mice displayed decreased locomotor activity within 5 to 10 minutes, with a partial resumption of locomotor activity within 2 to 4 hours. The grooming behavior of the mice returned to normal 3 days after injection. There was no change in locomotor activity or grooming behavior in the mice injected IP with diluent. As shown by the Kaplan-Meier analysis in **Figure 1A**, there was a statistically significant ($P = 0.025$) 14.3% decrease in survival in the ISO-treated mice, whereas there were no deaths in the diluent-treated mice. Treatment with ISO resulted in a significant increase in circulating levels of Troponin I at 1 hour ($P < 0.001$) and on day 1 ($P = 0.018$), but the levels were not different from baseline by day 2 (**Figure 1B**), Consistent with the increase in ISO-induced myocyte injury, there was a

FIGURE 2 LV Structure, Function, and Regional Wall Motion in a Model of Stress-Induced Cardiomyopathy

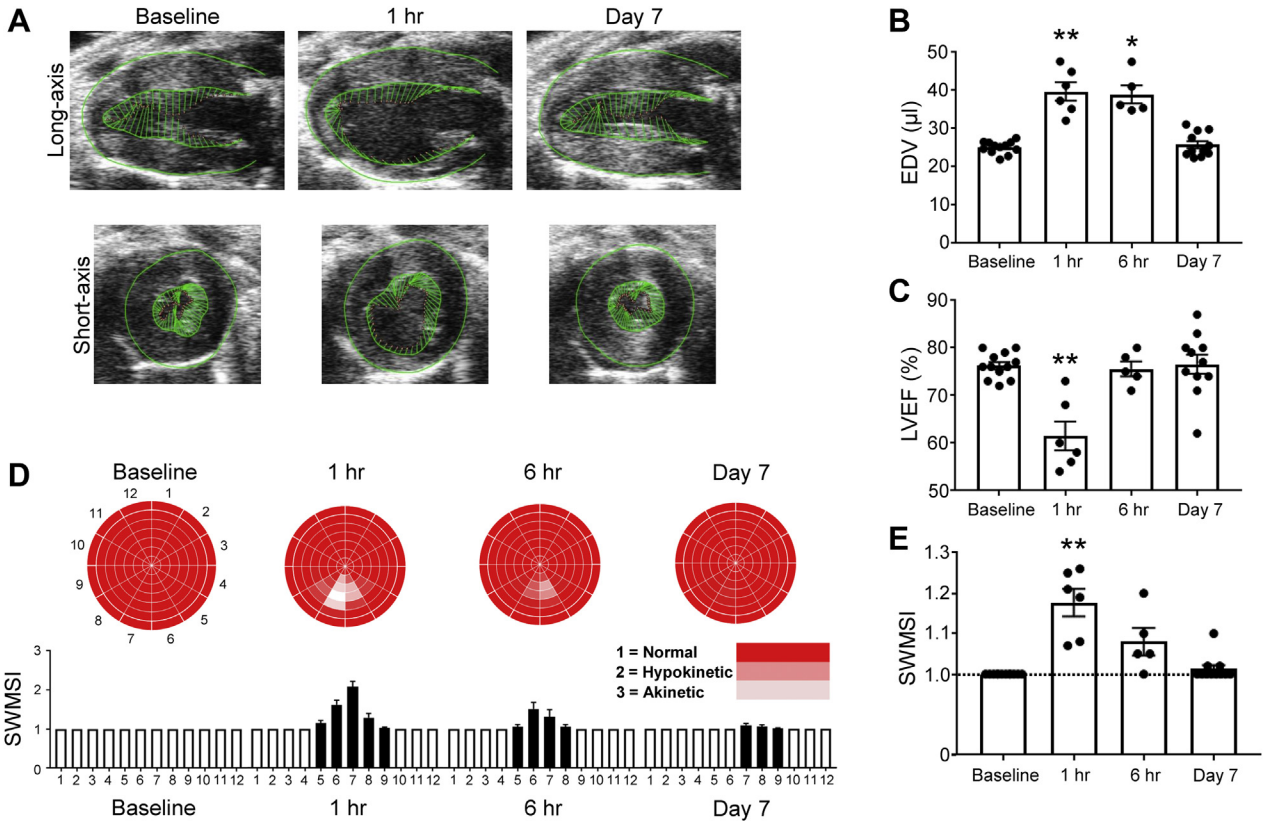

(A) Representative long-axis **(top)** and short-axis **(bottom)** 2-dimensional echocardiographic images from isoproterenol (ISO)-injected mice at baseline, 1 hour, and 7 days (see Videos S1 and S2). Superimposed **green lines** represent speckle-tracking analysis of endocardial and epicardial contours; radially oriented vectors represent the direction and amplitude of segmental endocardial velocities. **(B)** Left ventricular (LV) end-diastolic volume (EDV), **(C)** left ventricular ejection fraction (LVEF %), **(D)** regional segmental wall motion from LV base to apex, and **(E)** global segmental wall motion score index (SWMSI) at baseline, 1 and 6 hours, and 7 days after ISO injection (n = 5-12 mice/time). The global SWMSI was determined as the average of 84 regional LV segments, where 1 = normal wall thickening, 2 = hypokinesis, and 3 = akinesis. Data were analyzed by repeated measures 1-way analysis of variance with Dunnett's multiple comparisons relative to baseline. *$P < 0.05$; **$P < 0.01$.

significant increase in heart weight-to-tibia length on day 1 ($P = 0.040$) after ISO injection, which peaked on day 2 ($P = 0.013$) and returned to baseline levels by day 7 (Figure 1C).

To characterize the myocardial inflammatory response to ISO, we performed immunohistochemistry and FACS on diluent and ISO-treated hearts at 1 hour and on days 1, 2, 3, and 7. Figure 1D shows representative hematoxylin and eosin staining of leukocyte infiltrates on days 2 and 7 after ISO treatment; the results of group data are summarized in Figure 1F. The inflammatory score index was significantly greater on days 2 and 7 ($P < 0.001$ for both) in the ISO-treated mice when compared with baseline values. Masson's trichrome staining revealed that there was increased patchy fibrosis in the heart at 7 days after ISO injection (Figure 1E). Consistent with these findings, FACS analysis (Figure 1G) revealed that the number of $CD45^+$ leukocytes in the hearts increased significantly on days 2 ($P = 0.036$) and 3 ($P = 0.002$), and returned to baseline values incompletely by day 7 after ISO injection ($P < 0.001$ relative to baseline).

To determine whether the ISO-induced tissue injury resulted in changes in LV structure and function, we performed 2D echocardiography at baseline and at 3 sequential time points after ISO injection. Figure 2A shows representative 2D echocardiographic images of LV long- and short-axis structure at baseline, 1 hour, and 7 days after ISO injection (see also Videos S1 and S2), whereas group data are summarized in Figures 2B and 2C. ISO injection resulted in a significant increase in left ventricular end-diastolic volume (LVEDV) at 1 and 6 hours ($P = 0.004$ and

$P = 0.012$, respectively), with a return to baseline values by day 7. Left ventricular ejection fraction (LVEF) decreased significantly ($P = 0.005$) at 1 hour post-ISO injection, but normalized by 6 hours. To resolve whether ISO injection resulted in abnormalities in regional myocardial function, we performed a semiquantitative analysis of segmental wall motion after ISO injection. As shown in **Figure 2D**, treatment with ISO provoked segmental wall motion abnormalities in the mid to apical inferior wall of LV that were detectable as early as 1 hour after ISO injection. Although segmental wall motion abnormalities were still detectable in the mid to apical inferior wall of LV segments 6 hours after injection, the extent of segmental wall motion abnormalities was decreased relative to 1 hour. By 7 days, segmental wall motion abnormalities had normalized in most segments. As shown in **Figure 2E**, the SWMSI, which reflects the sum of all segmental wall motion abnormalities, was significantly worse ($P = 0.005$) at 1 hour after ISO injection, but was not significantly different from baseline values on day 7. Viewed together, these findings suggest that a single dose of ISO induces tissue injury and a brisk inflammatory response, which is accompanied by transient changes in LV structure and function that normalize within 7 days.

CHARACTERIZATION OF ISO-INDUCED INFLAMMATORY RESPONSE IN THE HEART, BLOOD, AND SPLEEN. Recognizing the reciprocal nature of the regulation between the adrenergic nervous system and the immune system,[15] we performed a comprehensive survey of the contemporaneous changes that occurred in subsets of immune cells residing in the heart, the circulation, and the spleen at baseline; at 1 hour after ISO injection; and on days 1, 2, 3, and 7 after ISO injection. The gating strategy for these separate FACS analyses are provided in Supplemental Figures 1 to 3.

Changes in the immune cell profile in the heart. As shown in **Figure 3A**, the number of $Ly6G^+$ neutrophils ($P = 0.001$) and $Ly6C^{high}CD64^{low}$ monocytes ($P = 0.031$) in the heart peaked on day 1 when compared with baseline values and remained significantly above baseline levels on day 7 ($P = 0.033$ and $P = 0.021$, respectively). The decline in monocytes in the heart was accompanied by a significant increase in the number of $CD64^+Ly6C^{low/-}$ macrophages, which were significantly elevated on day 3 ($P < 0.001$), partially returning to baseline values by day 7 ($P = 0.009$ relative to baseline) (**Figure 3F**). The number of $CD4^+$ T cells increased significantly in the heart on days 3 and 7 ($P = 0.014$ and $P = 0.004$, respectively), whereas the number of $CD8^+$ T cells did not become significantly ($P = 0.022$) elevated until day 7. In contrast, the number of $CD19^+$ B lymphocytes in the heart decreased significantly on days 1 ($P < 0.001$), 2 ($P = 0.007$), and 3 ($P = 0.008$), and returned to baseline values by day 7. Further analyses of profiles of B lymphocyte subsets revealed that the decrease in myocardial $CD19^+$ lymphocytes was secondary to a significant decrease in $CD19^+CD11b^-$ B2 cells (see Supplemental Figure S5). The response to ISO injury was qualitatively similar but quantitatively different in male mice. As shown in Supplemental Figure S6, although lethality was numerically greater in male mice, it was not significantly different than in female mice ($P = 0.223$). However, the extent of tissue injury and heart weight-to-tibia length was significantly greater in male mice when compared with female mice, and the inflammatory response was also significantly greater in male mice.

Changes in the cell profiles of circulating immune cells. The changes in the number of leukocytes in the blood were similar but not identical to those observed in heart after ISO injection. As shown in **Figure 3**, neutrophil number in the blood increased significantly at 1 hour ($P < 0.001$) and remained significantly elevated on day 7 ($P = 0.014$). The number of circulating $Ly6C^{high}CD64^{low}$ monocytes were not significantly different from baseline values at any of the other time points examined. Interestingly, ISO injection resulted in a numerical decrease in the number of circulating $CD4^+$ and $CD8^+$ T cells on days 1 and 2, with a return toward baseline values on days 3-7; the overall changes in cell numbers were not statistically significant for $CD4^+$ cells ($P = 0.175$ by ANOVA). Similar to the observations in the heart, the number of circulating B lymphocytes decreased significantly on days 1 ($P = 0.008$) and 2 ($P = 0.002$), which was secondary to a decrease in $CD19^+CD11b^-$ B2 cells (Supplemental Figure S5).

Changes in the cell profiles of splenic immune cells. Changes in the immune profile of splenic cells were expressed as the percentage of the total $CD45^+$ cells. The initial increase in the splenic neutrophils and monocytes on day 1 after ISO injection was similar but not identical to those observed in the in the heart. There was a significant increase in the percentage of $Ly6G^+$ ($P = 0.005$) and $Ly6C^{high}CD64^{low}$ ($P = 0.005$) cells on day 1 after ISO injection (**Figures 3A and 3B**), similar to what was observed in the heart. Consistent with our observations in the heart, the percentage of splenic $Ly6G^+$ neutrophils and $Ly6C^{high}CD64^{low}$ monocytes remained significantly elevated above baseline on day 7 ($P = 0.030$ and $P = 0.006$, respectively). There was no significant change in $CD4^+$ or $CD8^+$ T lymphocytes in the spleen at any time point after ISO injection. The percentage

FIGURE 3 Immunophenotyping of CD45$^+$ Cells in the Heart, Blood, and Spleen Following ISO Injection

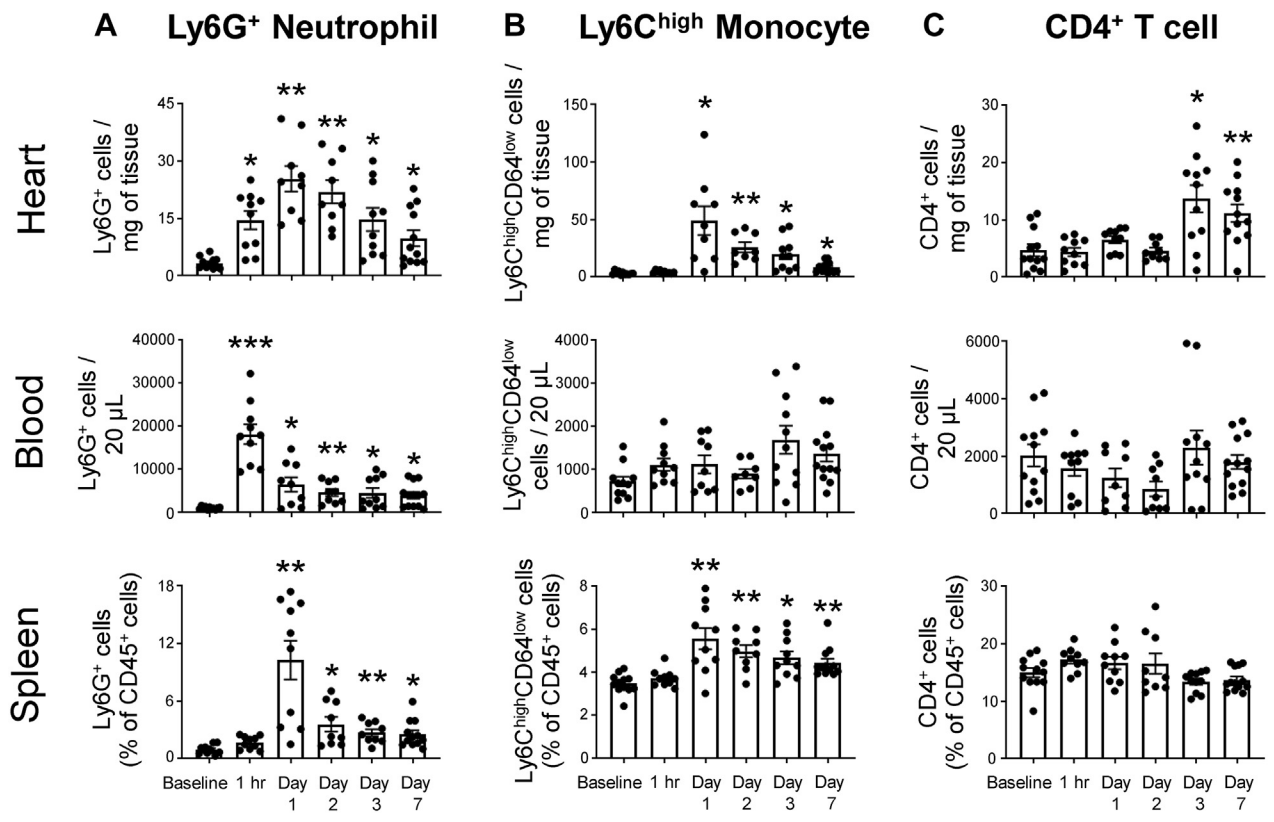

Flow cytometry was performed on CD45$^+$ cells that were isolated from the heart (cells/mg of tissue), blood (cells/20 µL) and spleen (% of CD45$^+$ cells) of identical mice. **(A)** Ly6G$^+$ neutrophils, **(B)** Ly6C^{high}CD64^{low} monocytes, **(C)** CD4$^+$ T cells, **(D)** CD8$^+$ T cells, and **(E)** CD19$^+$ B lymphocytes were isolated from the heart, blood, and spleen at baseline (n = 11-12 mice), 1 hour, and days 1-3 and 7 (n = 8-13 mice/time) after isoproterenol (ISO) injection. **(F)** CD64$^+$Ly6C$^{low/-}$ macrophages were isolated from the hearts of ISO-injected mice at baseline (n = 12 mice), 1 hour, and days 1-3 and 7 (n = 9-12 mice/time) after ISO injection. Data were analyzed by repeated measures 1-way analysis of variance with Dunnett's multiple comparisons relative to baseline. *$P < 0.05$; **$P < 0.01$; ***$P < 0.001$.

Continued on the next page

of CD19$^+$ B cells in the spleen decreased significantly ($P = 0.003$) on day 1 after ISO injection, with a return to baseline values on days 2, 3, and 7. Viewed together, these data suggest that ISO injection provokes time-dependent changes in immune-cell subsets in the heart that coincide temporally with the onset and resolution of myocardial injury. In contrast, the changes in immune-cell subsets in the blood and spleen were less pronounced than in the heart, and were not as tightly coupled to the time course of ISO-induced myocardial injury.

SINGLE-CELL RNA SEQUENCING. To further phenotype the changes in the immune-cell subsets in the heart following ISO injury, we performed single-cell RNA sequencing of CD45$^+$ leukocytes isolated from the heart at baseline and at days 2 and 7. As shown in by the Unsupervised Uniform Manifold Approximation and Projection plots in **Figure 4A**, we identified 10 distinct clusters of immune cells in the heart (see Supplemental Figure S7). At baseline, the most prominent cell clusters were B cells > LYVE1$^-$ macrophages (monocyte-derived tissue resident) > CCR2$^-$ LYVE1$^+$ macrophages (embryonic-derived tissue resident) = T cells = NK cells = dendritic cells = stromal cells > monocytes > granulocytes. Following ISO injury there was a striking increase in the cluster density of LYVE1$^-$ macrophages that was accompanied by increased cluster density for Ly6C$^+$ monocytes, granulocytes, dendritic cells, stromal cells and IFN activated macrophages. There was corresponding decrease in cluster density for B cells, T cells, NK cells, and CCR2$^-$LYVE1$^+$ macrophages. Following resolution of ISO injury, the cluster density

FIGURE 3 Continued

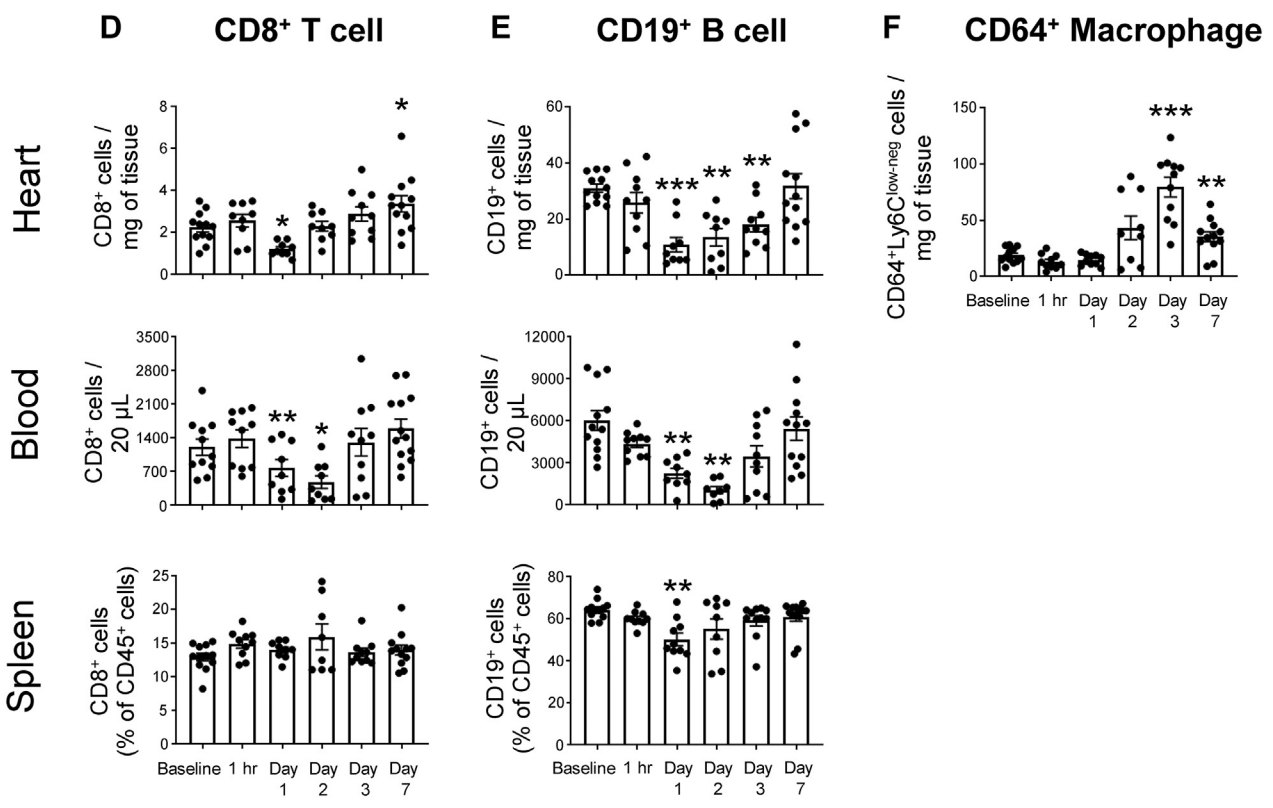

of LYVE1⁻ macrophages, dendritic cells, and IFN-activated macrophages remained elevated above baseline levels, whereas the relative cluster density of CCR2⁻LYVE1⁺ macrophages, stromal cells, granulocytes, and monocytes returned to baseline levels (**Figure 4B**). The cluster density of T cells, B cells, and NK cells on day 7 remained below baseline levels. The violin plot in **Figure 4C** shows that on day 2, the LYVE1⁻ macrophages, dendritic cells, and monocytes were CCR2⁺, suggesting that they were bone marrow derived.

To understand whether there were changes in the transcription profile of the different cell clusters, relative to baseline, we examined the differentially expressed genes (DEGs) profile in clusters 0-9 between baseline and 2 and between baseline and day 7 after ISO injury. Supplemental Table S3 shows that the greatest changes in gene expression in immune cells on day 2 were: LYVE1⁻ macrophages (1,879 DEGs) > monocytes (233 DEGs) > dendritic cells (156 DEGs) > CCR2⁻/LYVE1⁺ macrophages (65 DEGs) > IFN-activated macrophages (26 DEGs) > granulocytes (10 DEGs) > B cells (0 DEG) = T cells (0 DEG) = NK cells (0 DEG). The greatest changes in gene expression on day 7 in immune cells were: LYVE1⁻ macrophages (401 DEGs) > dendritic cells (15 DEGs) > CCR2⁻/LYVE1⁺ macrophages (11 DEGs) > IFN-activated macrophages (2 DEGs) > B cells (1 DEG) = T cells (1 DEG) > monocytes (0 DEG) = granulocytes (0 DEG) = NK cells (0 DEG).

We used a weighted gene network analysis (WGNA) to identify gene modules for DEGs in the LYVE1⁻ macrophages on days 2 and 7 relative to baseline levels (see Supplemental File S1 for gene lists). There were too few differentially expressed genes in the CCR2⁻/LYVE1⁺ and dendritic cell clusters to perform WGNA. Among the DEGs in LYVE1⁻ macrophages, WGNA revealed the emergence of 20 unique differentially expressed eigengene modules on day 2, and 7 differentially expressed eigengene modules on day 7. Prominent biological themes for eigengene modules on day 2 included neutrophil activation, increased glycolysis, antigen presentation, positive and negative regulation of cytokines and inflammation,

FIGURE 4 Single-Cell RNA Sequencing of CD45$^+$ Cells Isolated From the Heart Following ISO Injection

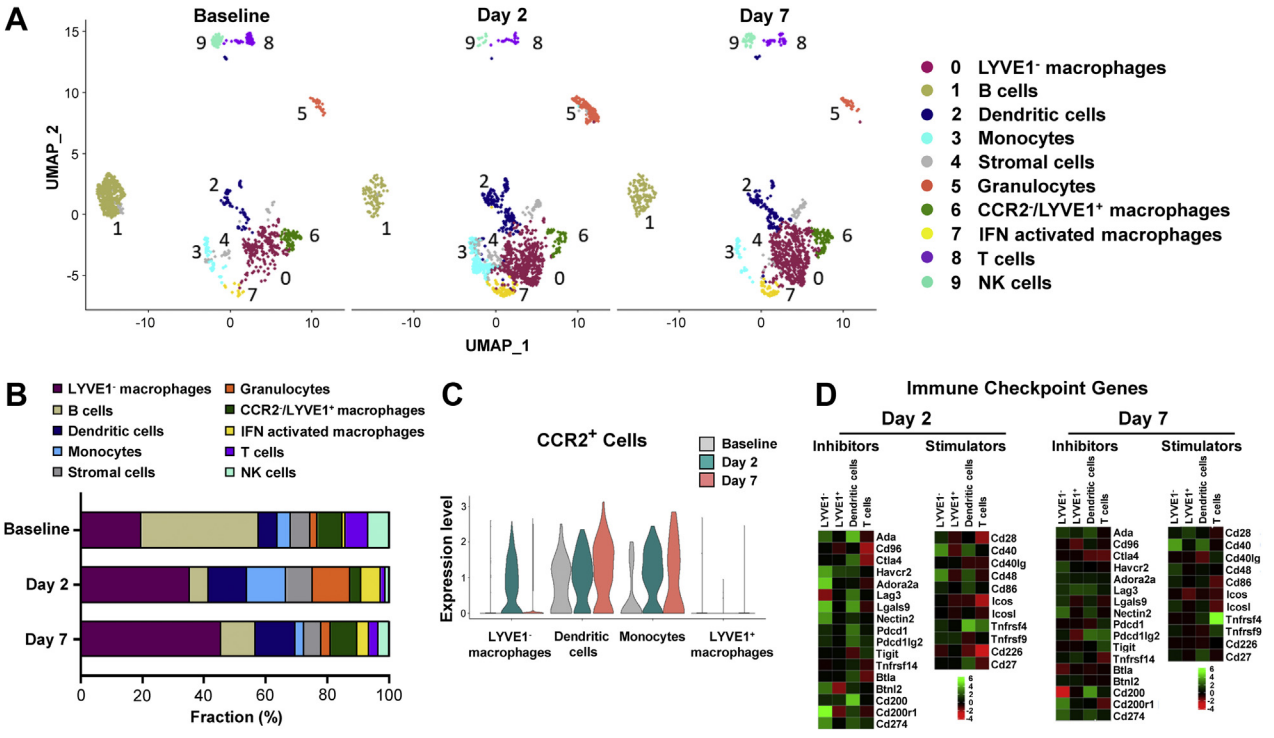

Unsupervised Uniform Manifold Approximation and Projection (UMAP) plot of 10× single-cell sequencing data from the total of 3,748 CD45$^+$ cells (baseline: 1,104 cells; day 2: 1,457 cells; day 7: 1,187 cells) after quality control. CD45$^+$ cells were sorted from the hearts of mice at baseline and on days 2 and 7 after isoproterenol (ISO) injection. **(A)** A total of 10 unique cell clusters were identified (see Methods) at each time period. **(B)** The proportion of cell clusters depicted in **A**. **(C)** Feature plot of CCR2$^+$ expression in LYVE1$^-$ macrophages, dendritic cells, monocytes, and LYVE1$^+$ macrophages. **(D)** Heat map of changes in gene expression for immune checkpoint inhibitors and stimulators in LYVE1$^-$ macrophages, LYVE1$^+$ macrophages, dendritic cells, and T cells. Data represent the fold change in expression levels (following log2 normalization) on days 2 and 7 relative to baseline.

changes in gene transcription and protein metabolism, and NF-κB signaling (Supplemental Figure S8A), whereas the prominent biological themes on day 7 included antigen presentation, phagocytosis, and T-cell regulation (Supplemental Figure S8B).

ISO-INDUCED INJURY UP-REGULATES THE PD-1/PD-L1/PD-L2 IMMUNE CHECKPOINT AXIS. Given the increasing recognition of the role of immune checkpoint molecules with respect to modulating immune responses, we examined the relative expression levels of inhibitory and stimulatory immune checkpoint genes in the LYVE1$^-$ macrophages, CCR2$^-$/LYVE1$^+$ macrophages, dendritic cells, and T-cell clusters shown in **Figure 4A**. As illustrated by the heat map in **Figure 4D**, the expression of inhibitory checkpoint genes, including *Pdcd1* (PD1), *Ada*, *Nectin2*, *Havcr2*, *Lgals9*, *Cd200r1*, *Btnl2*, and *Cd274* (PD-L1), were increased on day 2 after ISO injection relative to baseline levels. This was accompanied by a reciprocal decrease in the expression of immune checkpoint genes, such as *Cd28*, *Icos*, *Tnfrsf9*, *Cd27*, *Tigit*, *Btla*, *Cd226*, and *Cd40Ig* on day 2. By day 7 following ISO injury, the relative expression levels of 2 immune checkpoint inhibitory genes (*Havcr2*, *Lgals9*) were decreased, whereas several inhibitory immune checkpoint genes remained above baseline levels (*Pdcd1*, *Ada Nectin2*, *Cd200r1*, *Btnl2*, *Cd274*). Recognizing the role of the PD-1/PD-L1/PD-L2 signaling axis in the heart,[32] we explored the dynamics of the PD-1, PD-L1, PD-L2 protein expression in cardiac resident immune-cell subsets following ISO injury. As shown in Supplemental Figure S9A, there was a significant increase in the number of CD64$^+$, CD4$^+$, and CD8$^+$ cells expressing PD-1 and PD-L1 on day 2 after ISO injection, whereas increased PD-L2 expression was not detected in these cell types until

day 7. The expression levels of PD-1 returned to baseline values by day 7 in $CD64^+$, $CD4^+$, and $CD8^+$ cells, whereas the number of $CD64^+$ and $CD4^+$ cells expressing PD-L1 remained significantly above baseline levels on day 7 (gating strategy shown in Supplemental Figure S10).

To determine whether the dynamic regulation of the PD-1/PD-L1/PD-L2 axis was unique to immune cell subsets residing in the heart, we also performed a FACS analysis of immune cells in the blood (Supplemental Figure S9B) and the spleen (Supplemental Figure S9C). In contrast to the dynamic changes in the number of PD-1/PD-L1/PD-L2 expressing immune cells in the heart, there was no significant change in the number of $Ly6C^{high}CD64^{low}$ monocytes, $CD4^+$, and $CD8^+$ T cells expressing PD-1, PD-L1, or PD-L2 in the blood at any time point examined after ISO injection (gating strategy shown in Supplemental Figure S11). Surprisingly, there was no change in the percentage of PD-1^+ immune cells in the spleen at any time point examined, whereas there was an increase in the percentage of $Ly6C^{high}CD64^{low}$ cells expressing PD-L1 on day 2 and an increase in the percentage of $CD4^+$, $CD8^+$, and $CD19^+$ cells expressing PD-L1 on day 7. There was also an increase in the percentage of $CD19^+$ cells expressing PD-L2 on day 7 (gating strategy shown in Supplemental Figure S12). Viewed together, these data suggest that the ISO-induced cardiac injury increases the number of PD-1-, PD-L1-, and PD-L2-expressing macrophages and T cells at the site of tissue injury on days 2 and 7, with a delayed increase in the % of PD-L1- and PD-L2-expressing leukocytes in the spleen that occurred predominantly on day 7.

FUNCTIONAL SIGNIFICANCE OF PD-1/PD-L1/PD-L2 AXIS FOLLOWING MYOCARDIAL INJURY

The observation that the number of macrophages and T cells expressing PD-1, PD-L1, and PD-L2 increased in the heart and not in the circulation or spleen suggested that up-regulation of the PD-1/PD-L1/PD-L2 signaling axis in the heart modulated the inflammatory response following ISO injury. To test this possibility, we examined the ISO-induced inflammatory response in PD-$1^{-/-}$ mice and isogenic WT mice, as well as mice treated with anti-PD-1, anti-PD-L1, or PD-L2 Abs or isotype control Abs (**Figure 5A**). As shown by the Kaplan-Meier analysis in **Figure 5B**, there was no significant difference in the survival in the ISO-treated PD-$1^{-/-}$ mice in comparison to the WT mice, nor there was a difference in mortality in the mice treated with the anti-PD-1, anti-PD-L2, or isotype control Abs. There was, however, a striking 40% increase in mortality ($P = 0.005$) in the mice treated with the anti-PD-L1 Ab when compared with the isotype control or WT mice. **Figure 5C** shows that the troponin I levels were increased on day 2 in all groups of mice injected with ISO. However, the salient finding shown by **Figure 5C** is that the troponin I levels were significantly ($P = 0.047$) elevated in the mice treated with anti-PD-L1 Ab when compared with isotype control Ab-treated mice. The serum troponin I levels in PD-$1^{-/-}$ or anti-PD-1 Ab-treated WT mice were not significantly different from respective control WT mice on day 2, whereas serum troponin I levels were significantly higher on day 7 in the PD-$1^{-/-}$ mice ($P = 0.005$), but not in the anti-PD-1 Ab-treated mice, which may reflect differences in acute vs chronic attenuation of PD-1 signaling. Consistent with the increase in ISO-induced myocyte injury in WT mice treated with an anti-PD-L1 Ab, there was also a significant trend ($P = 0.079$) toward increase in heart weight-to-tibia length on day 2 in these mice relative to isotype control-treated mice, and a significantly greater increase in heart weight-to-tibia length at day 7 in the PD$1^{-/-}$ mice relative to WT mice ($P = 0.028$) (Supplemental Figure S13A).

To characterize the myocardial inflammatory response to ISO injection in PD-$1^{-/-}$ mice and in mice treated with anti-PD-L1 and anti-PD-L2 Abs, we performed immunohistochemical staining and FACS analysis. The inflammatory score index was significantly greater on day 2 ($P < 0.001$) after ISO injury in the mice treated with the anti-PD-L1 Ab when compared with isotype control Ab-treated mice, whereas the inflammatory score index was significantly greater ($P < 0.001$) on day 7 after ISO treatment in PD-$1^{-/-}$ mice relative to WT control mice (Supplemental Figures 13B and 13C). In accordance with these findings, relative to isotype-treated control mice, the number of myocardial $CD45^+$ cells were significantly increased on day 2 in the anti-PD-L1 Ab-treated mice ($P < 0.001$) and significantly increased on day 7 in the PD-$1^{-/-}$ mice ($P = 0.005$) relative to WT mice (**Figure 5D**).

To further delineate the immune response in subsets of $CD45^+$ leukocytes, we performed FACS analysis of $Ly6G^+$, $Ly6C^{high}CD64^{low}$ monocytes, $CD64^+$ macrophages, $CD4^+$ T cells, $CD8^+$ T cells, and $CD19^+$ B cells in the heart, blood, and spleen in WT and PD-$1^{-/-}$ mice, and anti-PD-1, anti-PD-L1, anti-PD-L2 Abs, and isotype Ab control-treated WT mice at baseline and at days 2 and 7 after ISO injury. As shown in **Figures 5E to 5J**, relative to the respective control mice, there was no significant increase in the number of $Ly6G^+$, $Ly6C^{high}CD64^{low}$, $CD64^+$, $CD4^+$, and $CD19^+$ cells in the heart on day 2 after ISO

FIGURE 5 Effects of ISO Injury in PD-1$^{-/-}$ Mice and WT Mice Injected With Anti-PD-1, Anti-PD-L1, and Anti-PD-L2 Monoclonal Abs

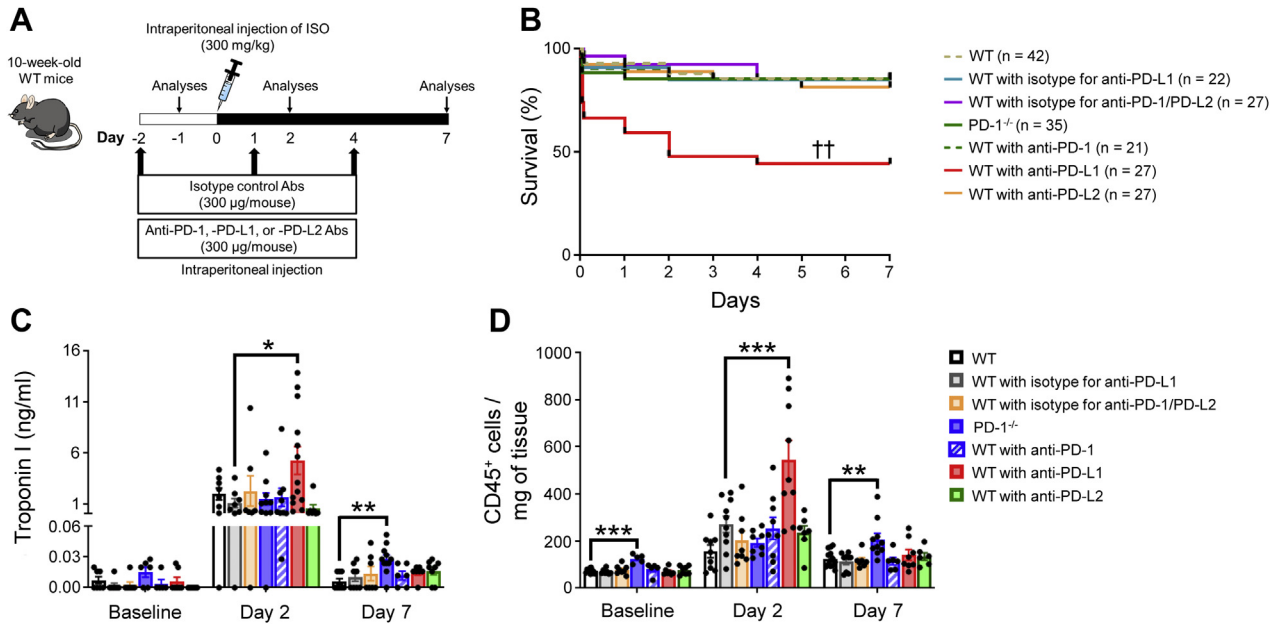

(A) Experimental protocol for isoproterenol (ISO)-injected mice treated with anti-PD-1, anti-PD-L1, anti-PD-L2 antibodies (Abs), or isotype control Abs. **(B)** Kaplan-Meier survival curves of ISO-injected wild-type (WT), PD-1$^{-/-}$ mice, or ISO-treated WT mice injected with anti-PD-1, anti-PD-L1, anti-PD-L2 Abs, or isotype control Abs. **(C)** Serum troponin I levels at baseline, day 2 and day 7 in ISO-injected WT, PD-1$^{-/-}$ mice or ISO-treated WT mice injected with anti-PD-1, anti-PD-L1, anti-PD-L2 Abs or isotype control Abs (n = 5-13 mice/group/time). **(D)** Flow cytometry analysis of the number of CD45^{+} cells/mg of heart tissue. Number (cells/mg of heart tissue) of **(E)** Ly6G^{+} neutrophils, **(F)** Ly6C^{high}CD64^{low} monocytes, **(G)** CD64^{+}Ly6C$^{low/-}$ macrophages, **(H)** CD4^{+} T cells, **(I)** CD8^{+} T cells, and **(J)** CD19^{+} B lymphocytes in ISO-injected WT, PD-1$^{-/-}$ mice, or ISO-treated WT mice injected with anti-PD-1, anti-PD-L1, anti-PD-L2 Abs, or isotype control Abs (n = 4-13 mice/group/time). Data were analyzed by 1-way analysis of variance with Tukey's multiple comparisons within each time point **(C to J)**. *$P < 0.05$; **$P < 0.01$; ***$P < 0.001$; ††$P < 0.01$ relative to isotype control.

Continued on the next page

injection in the PD-1$^{-/-}$ mice or mice treated with an anti-PD-1 Ab, whereas there was a trend ($P = 0.065$) toward significance in the number of CD8^{+} lymphocytes in the anti-PD-1 Ab mice. In contrast to the kinetics of the immune cell response observed in the PD-1$^{-/-}$ mice and anti-PD-1 Ab-treated mice, there was a significant increase in the Ly6G^{+} ($P < 0.001$), Ly6C^{high}CD64^{low} ($P = 0.029$), CD4^{+} ($P = 0.009$), and CD8^{+} ($P = 0.029$) cells on day 2 in the anti-PD-L1 Ab-treated mice relative to isotype control Ab-treated mice. Intriguingly, on day 7 after ISO injection there was a significant increase in the number of CD64^{+} ($P = 0.001$), CD4^{+} ($P < 0.001$), and CD8^{+} ($P = 0.003$) cells in the hearts of the PD-1$^{-/-}$ mice, consistent with a delayed inflammatory response in these mice, whereas the inflammatory response was almost completely resolved in the WT mice treated with anti-PD-1 Ab or anti-PD-L1 Ab, save for a small but significant increase in Ly6C^{high}CD64^{low} ($P = 0.024$) cells in the anti-PD-L1 Ab-treated mice. Treatment with an anti-PD-L2 Ab had no effect on the number of immune cells in the ISO-injured heart on either day 2 or 7. Viewed together these data indicate that initial magnitude of the inflammatory response is greater in mice treated acutely with an anti-PD-L1 Ab, whereas mice with a germ line deletion of PD-1 have a prolonged inflammatory response following tissue injury.

Given the central role of ICIs in regulating T cells, we asked whether the observed increase in CD4^{+} and CD8^{+} T cells in PD-1$^{-/-}$ mice was responsible for the delayed resolution of inflammation and increased tissue injury observed in the PD-1$^{-/-}$ mice on day 7. As shown in Supplemental Figure S14A, we pretreated PD-1$^{-/-}$ mice with CTLA4Ig (to prevent T-cell activation) 2 days before ISO injection, as well as on days 1 and 4 after ISO injection. Mice treated at identical time points with an isotype control Ab served as the appropriate controls. PD-1$^{-/-}$ mice injected with CTLA4Ig had a significant reduction in the number of CD4^{+} and CD8^{+} T cells on day 7 after ISO injury, as well as in the number of

FIGURE 5 Continued

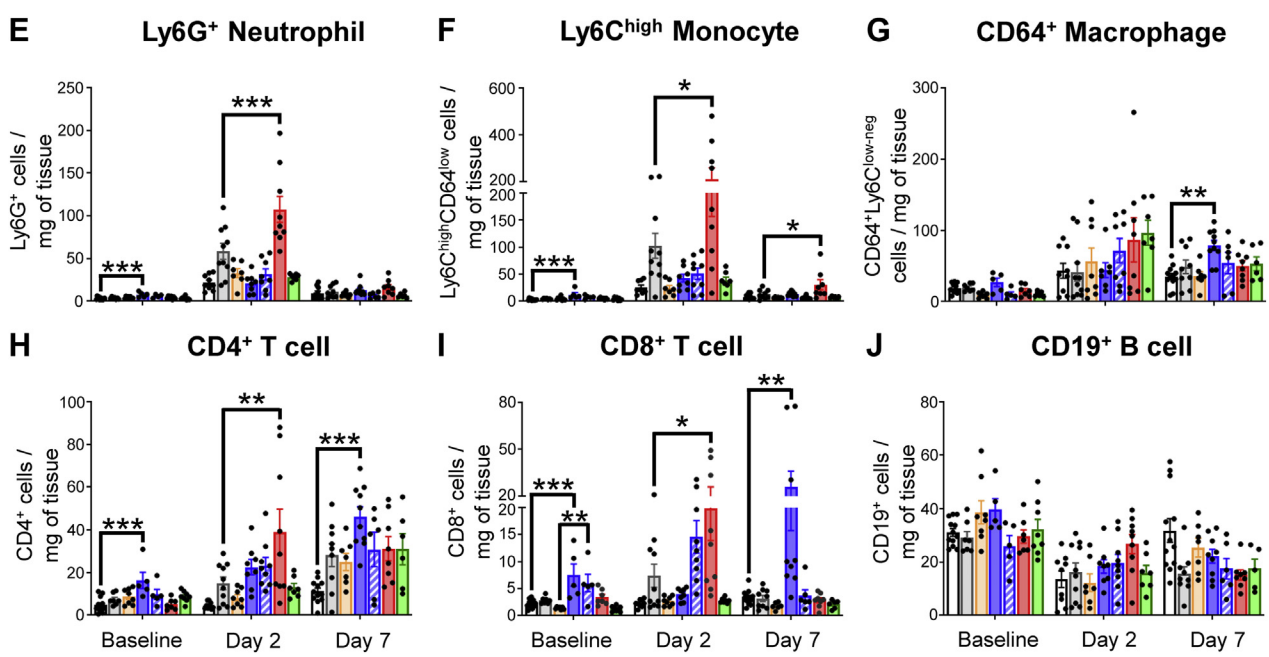

$CD4^+CD62L^-CD44^-$ and $CD8^+CD62L^-CD44^-$ effector T cells, when compared with the isotype control Ab-treated PD-$1^{-/-}$mice (Supplemental Figures S14B and S14C). However, the troponin I levels in the ISO-injected mice on day 7 were not different in the CTLA4Ig-treated mice relative to isotype control mice (Supplemental Figure S14D), nor did blocking T-cell activation with CTLA4Ig result in a decrease the number of $CD45^+$ (Supplemental Figure S14E), $Ly6G^+$, $Ly6C^{high}CD64^{low}$, $CD64^+$, and $CD19^+$ cells on day 7 (Supplemental Figure S14F), suggesting that the delayed resolution of inflammation and increased tissue injury in the PD-$1^{-/-}$ mice was not dependent on activation of T cells.

We also immunoprofiled ISO-induced changes in immune cells in the blood and the spleen of PD-$1^{-/-}$ mice and mice treated with anti-PDL-1 and anti-PD-L2 Abs (Supplemental Figure S15). Of note, at baseline there were significant increases in the number of circulating $CD4^+$ cells ($P < 0.001$), $CD8^+$ cells ($P < 0.001$), and $CD19^+$ cells ($P = 0.010$) in the PD-$1^{-/-}$ mice relative to WT mice, whereas there were no differences in the percentage of splenic $CD4^+$, $CD8^+$, or $CD19^+$ cells in the PD-$1^{-/-}$ mice at any time point examined. Following ISO injury, the number of circulating $CD19^+$ cells was significantly ($P < 0.001$) greater on day 2 after ISO injury in the PD-$1^{-/-}$ mice when compared with WT mice, whereas $Ly6G^+$ cells were greater in the circulation ($P = 0.009$) and the spleen ($P < 0.001$) in the PD-$1^{-/-}$ mice on day 7. In contrast, treatment with anti-PD-L1 or PD-L2 Abs had no effect on ISO-induced changes in circulating or splenic immune cells at any time point that was examined.

To ascertain whether the delayed resolution of inflammation in the PD-$1^{-/-}$ mice resulted in changes in LV structure and function, we performed 2D echocardiography in the PD-$1^{-/-}$ mice at baseline as well as 1 hour, 6 hours, and 7 days after ISO injection. ISO-induced cardiac injury resulted in a significantly greater increase in LVEDV at 1 hour ($P = 0.001$) and 6 hours ($P = 0.007$) in PD-$1^{-/-}$ mice relative to WT (**Figure 6B**). Although the initial decline in LVEF was similar in the WT and PD-$1^{-/-}$ mice 1 hour after ISO injection, the LVEF normalized in the WT mice 6 hours after ISO injection, whereas the LVEF remained significantly ($P = 0.005$) depressed in the PD-$1^{-/-}$ mice at 6 hours (**Figure 6C**). Both LVEDV and LVEF were not significantly different between WT and PD-$1^{-/-}$ mice at 7 days. The number of ISO-induced segmental wall motion abnormalities in the mid to apical inferior segments of the LV were similar in WT and PD-$1^{-/-}$ mice at 1 hour, but numerically greater in the PD-$1^{-/-}$ mice at 6 hours ($P = 0.015$) and on day 7 ($P = 0.318$), when compared with ISO-injected WT control mice (**Figures 6A and 6D**).

FIGURE 6 LV Structure, Function, and Regional Wall Motion in PD-1$^{-/-}$ Mice After ISO Injection

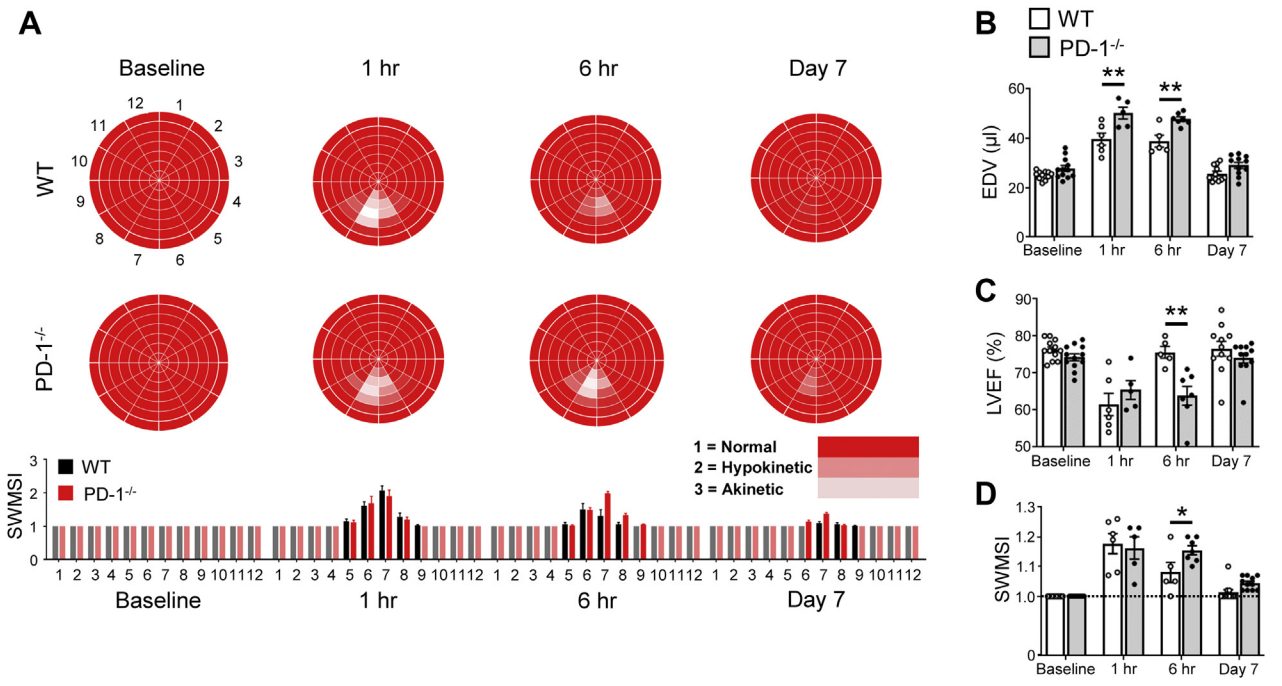

(A) Regional segmental wall motion from left ventricular (LV) base to apex in wild-type (WT) mice (data from Figure 2D were reproduced here for ease of comparison) and PD-1$^{-/-}$ mice at baseline, 1 and 6 hours, and 7 days after isoproterenol (ISO) injection (n = 5-12 mice/group/time). **(B)** LV end-diastolic volume (EDV), **(C)** left ventricular ejection fraction (LVEF %), and **(D)** global segmental wall motion score index (SWMSI) at baseline, 1 and 6 hours, and 7 days after ISO injection (n = 5-12 mice/group/time). The global SWMSI was determined as the average of 84 regional LV segments, where 1 = normal wall thickening, 2 = hypokinesis, and 3 = akinesis. Data were analyzed by repeated measures 2-way analysis of variance With Sidak's multiple comparisons **(B to D).** *$P < 0.05$; **$P < 0.01$.

NECROTIC MYOCARDIAL CELL EXTRACTS INCREASE THE PERCENTAGE OF PD-1^{+} INFLAMMATORY CELLS THROUGH TLR SIGNALING. To gain insights into the mechanism(s) responsible for the up-regulation of PD-1 in immune cells in the heart following ISO injury, we stimulated peritoneal derived immune cells (PDICs) with NCEs in vitro to mimic the immune cell activation provoked by the release of damage-associated molecular patterns by necrotic cells. We have shown previously that NCEs initiate a brisk inflammatory response in the heart through engagement of TLR4.[27] As shown in Figures 7A to 7C, stimulation of PDICs with NCEs provoked a significant increase in the percentage of PD-1-expressing CD64^{+} macrophages ($P < 0.001$), CD4^{+} ($P < 0.001$), and CD8^{+} ($P < 0.001$) T lymphocytes. The percentage of CD64^{+}, CD4^{+}, and CD8^{+} cells expressing PD-1 was similar in cells treated with NCEs or Pam3CSK4, a TLR2 agonist. In contrast, LPS, a (TLR4 agonist) significantly increased the percentage of CD64^{+} cells expressing PD-1, but did not increase the percentage of PD-1^{+}CD4^{+} and PD-1^{+}CD8^{+} cells. Importantly, ISO had no effect on PD-1 expression in isolated CD64^{+} macrophages, CD4^{+}, and CD8^{+} T lymphocytes (Figures 7D to 7F). To further investigate the role of TLR-mediated signaling and the relevant downstream signaling pathway triggered by NCEs, we pretreated NCE-stimulated PDIC cultures with anti-TLR2/4 blocking Abs or IMD-0354 (IKKβ/NF-kB inhibitor) (Figures 7G to 7I). Treatment with an anti-TLR2 Ab abolished the NCE-induced increase in the percentage of CD64^{+}, CD4^{+}, and CD8^{+} cells expressing PD-1, whereas treatment with an anti-TLR4 Ab abolished the NCE-induced increase in the percentage of CD64^{+} and CD4^{+} T cells expressing PD-1, but had no effect in CD8^{+} T lymphocytes. Importantly, pretreating the PDIC cultures with IMD-0354 to inhibit NF-κB signaling abrogated the NCE-induced increase in the percentage of CD64^{+}, CD4^{+}, and CD8^{+} T cells expressing PD-1. Viewed together, these findings suggest that NCEs are

FIGURE 7 **Damage-Associated Molecular Patterns Provoke PD-1 Up-Regulation Through the NF-κB-Dependent TLR Signaling Pathway in Peritoneum-Derived Macrophages and T Lymphocytes**

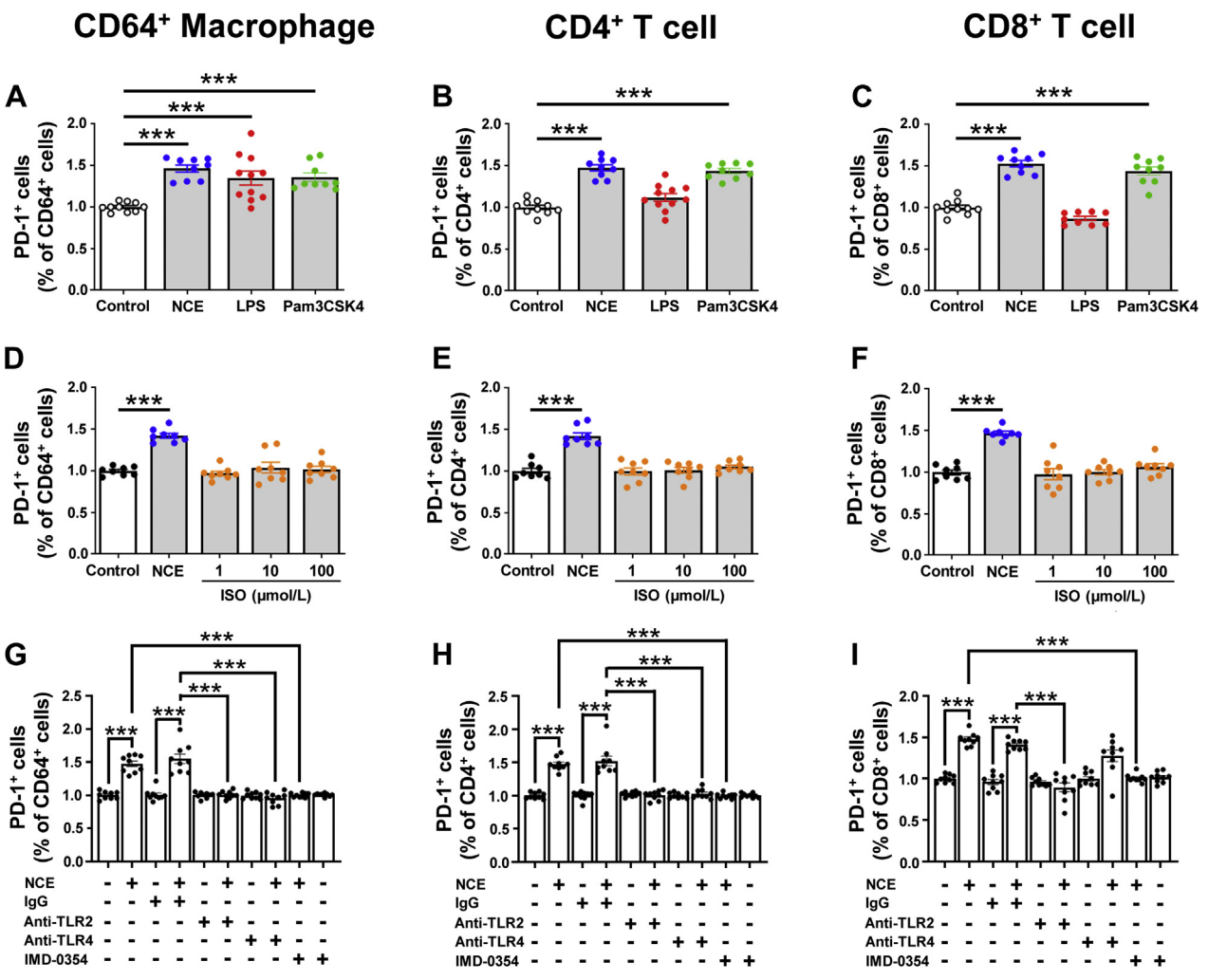

Unfractionated peritoneum-derived inflammatory cells (PDICs) were collected following 72-hour culture and the percentage of PD-1$^+$CD64$^+$ macrophages, PD-1$^+$CD4$^+$, and PD-1$^+$CD8$^+$ T lymphocytes was evaluated by flow cytometry analysis. **(A to F)** PDICs were cultured in media alone (control) or necrotic cardiac myocyte cell extracts (NCEs) (10 μg/mL), a Toll-like receptor 2 (TLR2) agonist (Pam3CSK4; 200 ng/mL), a TLR4 agonist (lipopolysaccharide [LPS]; 100 ng/mL), or isoproterenol (ISO) (1, 10, or 100 μmol/L). PD-1 expression in **(A)** CD45$^+$Aqua$^-$CD64$^+$ macrophages (n = 9-11 biological replicates/group), **(B)** CD45$^+$Aqua$^-$CD4$^+$ T lymphocytes (n = 9-11 biological replicates/group), **(C)** CD45$^+$Aqua$^-$CD8$^+$ T lymphocytes (n = 9-10 biological replicates/group), **(D)** CD45$^+$Aqua$^-$CD64$^+$ macrophages (n = 8 biological replicates/group), **(E)** CD45$^+$Aqua$^-$CD4$^+$ T lymphocytes (n = 8 biological replicates/group), and **(F)** CD45$^+$Aqua$^-$CD8$^+$ T lymphocytes (n = 8 biological replicates/group). **(G to I)** PDICs were cultured in media alone (control) or in the presence or absence of NCEs (10 μg/mL), IgG (4 μg/mL), anti-TLR2 antibody (Ab) (4 μg/mL), anti-TLR4 Ab (10 μg/mL), or NF-κB inhibitor (IMD-0354; 1 μmol/L). The percentage of cells expressing PD-1 was determined for **(G)** CD45$^+$Aqua$^-$CD64$^+$ macrophages (n = 9 biological replicates/group), **(H)** CD45$^+$Aqua$^-$CD4$^+$ T lymphocytes (n = 9 biological replicates/group), and **(I)** CD45$^+$Aqua$^-$CD8$^+$ T lymphocytes (n = 9 biological replicates/group). Data are expressed as fold changes relative to control values and presented as mean ± SEM, and were analyzed by 1-way analysis of variance with Tukey's multiple comparisons. ***$P < 0.001$.

sufficient to increase the percentage of CD64$^+$ and CD4$^+$ cells expressing PD-1 through a TLR2/TLR4/NF-κB-dependent manner in macrophages and CD4$^+$ T lymphocytes, whereas the effect of NCEs in CD8$^+$ T lymphocytes is mediated through TLR2/NF-κB dependent pathway.

DISCUSSION

We performed an in-depth phenotypic characterization of the time-dependent changes in cardiac resident immune cells, circulating immune cells, and splenic immune cells in an experimental model of

reversible stress-induced cardiomyopathy. Here, we show that transient myocardial injury induced by a neurohormonal stress provokes an acute inflammatory response that is accompanied by reversible changes in LV structure and function, and that inhibitory immune checkpoint receptors and ligands belonging to the PD-1:PD-L family are responsible, at least in part, for modulating the acute myocardial inflammatory response, as well as normalization of stress-induced abnormalities of LV structure and function. The following 3 lines of evidence support these statements.

First, ISO injection resulted in a transient release of troponin I (**Figure 1B**) and a self-limited myocardial inflammatory response that occurred *pari passu* with increased myocardial tissue edema (**Figure 1C**), inferoapical regional LV wall motion abnormalities (**Figures 2A and 2D**), increased LV dilation (**Figure 2B**), and decreased LV function (**Figure 2C**). The changes in myocardial structure and function normalized with the resolution of the inflammatory response (**Figures 1F, 1G, and 2**). Second, phenotypic analysis of the response of immune cells in the heart following transient myocardial injury was in overall agreement with the temporal pattern of immune cell trafficking observed following acute myocardial infarction, namely an early influx of $Ly6G^{+}$ neutrophils and $Ly6C^{high}CD64^{low}$ monocytes early after tissue injury, followed by an increase in the population of $CD64^{+}Ly6C^{low/-}$ macrophages and $CD4^{+}$ and $CD8^{+}$ T cells at later time points after tissue injury (**Figure 3**).[33] The decrease in myocardial $CD19^{+}$ B cells following ISO injury differs from the increase in myocardial B cells that has been reported following acute myocardial infarction or ischemia reperfusion injury.[26,34] Single-cell RNA sequencing of immune cell populations in the heart revealed that tissue injury stimulated the expansion of $LYVE1^{-}$ macrophage and dendritic cell clusters, as well as the emergence of a unique cluster of IFN activated macrophages (**Figure 4**), suggesting that resolution of the inflammatory response was accompanied by phenotypic changes in the immune cell clusters in the heart relative to the phenotype of immune cell clusters in naïve hearts. WGNA further suggested that the transcriptional profile of the $LYVE1^{-}$ macrophage cell clusters is functionally different after resolution of tissue injury and inflammation, with up-regulation of biological themes related to antigen presentation, phagocytosis, and T-cell regulation.

Third, acute tissue injury provoked an increase in inhibitory immune checkpoint genes along with a down-regulation of stimulatory immune checkpoint genes (**Figure 4D**) in $LYVE1^{-}$ and $LYVE1^{+}$ macrophages, and dendritic cell clusters (**Figure 4D**). Surprisingly, we observed minimal changes in the expression levels of immune checkpoint genes in T-cell clusters (**Figure 4D**). The stress-induced up-regulation of the PD-1/PD-L1/PD-L2 axis in cardiac resident $CD64^{+}$, $CD4^{+}$, and $CD8^{+}$ immune cells on day 2 after ISO-induced injury was tissue autonomous, insofar as the up-regulation of these immune checkpoint proteins did not occur until day 7 after tissue injury in subsets of circulating and splenic immune cells. Consistent with this point of view, necrotic cardiac extracts were sufficient to increase the number of $PD\text{-}1^{+}$ $CD64^{+}$, $CD4^{+}$, and $CD8^{+}$ cells in vitro (**Figure 7**). The observation that the ISO-induced inflammatory response did not completely resolve in $PD\text{-}1^{-/-}$ mice and that the sustained inflammation was associated with persistent myocardial edema (Supplemental Figure S13A) and delayed resolution of adverse LV remodeling structure and depressed LV function relative to WT control mice (**Figures 6B and 6C**), coupled with the finding that the magnitude of the ISO-induced inflammatory response was increased in mice treated with an anti-PD-L1 Ab and resulted in a 40% increase in mortality in these mice relative to isotype-treated control mice, suggests that the observed changes in the PD-1/PD-L1 axis in cardiac resident immune cells following tissue injury are functionally significant. Viewed together, these studies suggest a previously unappreciated role for immune checkpoints in regulating myocardial homeostasis following tissue injury.

Our findings with respect to the rapid onset and rapid resolution of cardiac injury and inflammation in WT mice are consistent with the known pharmacokinetics of ISO (half-life 4-5 minutes[35]), the reported kinetics of troponin release (24 hours) and normalization of troponin levels (48 hours) after ISO injection,[36-38] and the rapid recovery of LV function following ISO injury (see Supplemental Table S4).[39,40] Our results differ from a recent study by Liao et al[41] who reported that inflammation and elevated troponin levels persisted for up to 1 week in female mice injected with a single dose of ISO (200 mg/kg IP). Histological sections of the mouse hearts revealed fibrosis and cell death at 1 week after ISO injection.[41] Although the reason(s) for the discrepancy between this and prior studies and the report by Liao et al[41] are not clear, they may relate, at least in part, to differences in the technique for injecting ISO IP, which can lead to transient hypotension[42] and increased gut permeability.[43] In our early studies with this model, we observed that mice that did not resume normal locomotor activity and developed a hunched posture and ruffled for 3-7 days after ISO injection also lost

body weight and developed profound lymphopenia, and were distinctly different biologically from mice that recovered rapidly following ISO injection. With refinements in the ISO injection technique, we observed that the majority of ISO-injected animals recovered completely, consistent with what has been observed in patients with stress-induced cardiomyopathy.

IMMUNE CHECKPOINTS AND MYOCARDIAL TISSUE HOMEOSTASIS. PD-1 is a type I transmembrane protein that belongs to the CD28 superfamily of immune-regulatory receptors that also includes CTLA4. PD-1 was initially identified on the cell surface of activated T lymphocytes, and can be inducibly expressed on B cells, monocytes, macrophages, and dendritic cells.[44] Interactions between PD-1 and its cognate ligands, PD-L1 and PD-L2, restrain T-cell activity by inhibiting antigen-mediated T-cell receptor signaling pathways. PD-L1 is broadly expressed, and is inducible in B cells, dendritic cells, and macrophages, as well as in some nonhematopoietic cells such as epithelial and endothelial cells, as well as cardiac myocytes.[45-47] PD-L2 has more limited expression and is mainly restricted to antigen-presenting cells, such as subsets of B cells, macrophages, and dendritic cells. Although the vast majority of research on immune checkpoints has focused on the importance of these molecules in regulating T-cell activation, the studies presented herein along with recent studies in the cancer literature serve to highlight the importance of the role of immune checkpoints in regulating innate immune responses as well.[45] Indeed, when we treated PD-1$^{-/-}$ mice with a CTLA4Ig to prevent T-cell activation, we did not observe a decrease in ISO-induced tissue injury or a decrease in the inflammatory response relative to isotype control-treated mice, suggesting that the increased tissue injury in the ISO-treated PD-1$^{-/-}$ mice was mediated by innate immune cells (Supplemental Figures S14D and S14E). Finally, although checkpoint inhibitory ligands are predominantly thought to exert their effects by engaging inhibitory T-cell receptors in *trans*, some of the effects of immune checkpoint receptor ligand interactions may result from ligands that are able to engage costimulatory T-cell molecules in *cis* (ie, within the same cell).[45] For example, PD-L1 has been shown heterodimerize with CD80 (B7-1) on the surface of dendritic cells, thereby disrupting trans PD-L1:PD-1 interactions with immune cells.[48,49] Accordingly, blocking PD-L1 may have different effects on immune cell interactions than blocking PD-1.[45] Whether these observations explain, at least in part, the observed differences in outcomes from blocking PD-1 and PD-L1 in the ISO-injured mice is not known and will require further study.

Much of what is known about the PD-1:PD-L immune checkpoint signaling axis in the heart has been gleaned indirectly from studies on myocarditis, vasculitis, and pericarditis in cancer patients undergoing treatment with ICI therapies (reviewed by Varricchi et al[32]). Relevant to this discussion, stress-induced cardiomyopathy has been also reported in patients receiving ICIs.[50] The observation that ICI myocarditis in patients is characterized by myocardial infiltration of macrophages and T lymphocytes and is associated with cardiac myocyte death and LV dysfunction[32] is entirely consistent with the experimental observations in the present study, wherein we observed that inhibition of the PD-1/PD-L1 immune checkpoint axis resulted in a prolonged inflammatory response and cardiac myocyte death in response to a superimposed transient neurohormonal stress. Although the mechanism of ICI-induced myocarditis is not clearly known and has been attributed to disruption of cellular tolerance and or cross-reactivity to tumor antigens resulting in infiltration of T lymphocytes and monocytes and macrophages,[51] the results of the present study suggest an alternative, albeit not mutually exclusive possibility: ICI-induced myocarditis may arise, at least in part, because of the inability to dampen the normal physiological inflammatory responses that facilitate tissue repair in the heart,[1] which is continually exposed to mechanical stress and strain as well as high levels of reactive oxygen species. Conceptually, the failure to resolve physiological inflammatory responses in the heart would lead to increased myocardial injury, dendritic cell activation, and T-cell priming with cardiac specific peptides in the secondary lymphoid tissue that drain the heart, with the result that activated circulating T-cell clones would rapidly expand when they re-encounter tissue specific antigens in the heart.

CONCLUSIONS

The clinical success with ICIs across a variety of solid and hematological malignancies has highlighted the central role of T cells in cancer immunotherapy. Although there is increasing recognition that immune checkpoints regulate innate immune cells, the focus of these studies has been in the context of understanding how immune checkpoint blockade affects the antitumor response of innate immune cells.[45] Here, we show that transient myocardial tissue injury up-regulates the PD-1:PD-L signaling axis in cardiac resident innate immune cells, and that the disruption of this axis increases and prolongs the

myocardial inflammatory response, resulting in increased collateral tissue damage and delayed normalization of LV structure and function. Viewed together, these studies expand the role of immune checkpoint biology beyond that of modulating T-cell responsiveness in malignancies, and highlight a previously unappreciated role for immune checkpoints as essential components of the tightly integrated biological process for resolving acute myocardial inflammation and restoring tissue homeostasis. Whether these observations are relevant to the development of pathological inflammatory responses in the hearts of patients who are being treated with ICIs is unknown and will require additional studies. Aside from the importance of these studies in terms of our understanding the regulation of physiological inflammation in the heart, they also raise the interesting possibility that immune checkpoint agonists might be exploited therapeutically in conditions where there are dysregulated immune responses, including autoimmune diseases, acute graft rejection, giant cell myocarditis, and neuroinflammation.[52,53]

PERSPECTIVES

COMPETENCY IN MEDICAL KNOWLEDGE: Despite the increasing number of cancer patients and survivors treated with ICIs, the mechanisms of ICI-induced myocarditis or functions of immune checkpoints in the heart remain unclear. Our study highlights the role of immune checkpoint biology in regulating innate immune responses beyond the T-cell and an important role of immune checkpoints in resolving acute myocardial inflammation and restoring tissue homeostasis.

TRANSLATIONAL OUTLOOK: Our experimental findings are entirely consistent with the features of human ICI-associated myocarditis, such as myocardial infiltration of macrophages and T lymphocytes, cardiac myocyte death, and LV dysfunction. Considering that cancer patients are often exposed to environmental stress, ICI-associated myocarditis may be, at least in part, attributable to the inability to dampen the normal physiological inflammatory responses that facilitate cardiac tissue repair. Further studies are needed to determine whether our observations are relevant to the development of pathological myocardial inflammatory responses in patients treated with ICIs. The present study also provides the basis for a translational strategy that immune checkpoint agonists might be exploited therapeutically in immune dysregulation disorders, such as autoimmune diseases, acute graft rejection, giant cell myocarditis, and neuroinflammation.

FUNDING SUPPORT AND AUTHOR DISCLOSURES

This study was supported by research funds from the National Institutes of Health (R01HL147968, R01 HL155344, and S10 OD028597) the Veterans Administration (AN # 4345132), and the Wilkinson Foundation and Elissa and Paul Cahn. The authors have reported that they have no relationships relevant to the contents of this paper to disclose.

ADDRESS FOR CORRESPONDENCE: Dr Douglas L. Mann, Center for Cardiovascular Research, 660 South Euclid Avenue, Campus Box 8086, St. Louis, Missouri 63110, USA. E-mail: dmann@wustl.edu.

REFERENCES

1. Medzhitov R. Origin and physiological roles of inflammation. *Nature*. 2008;454:428–435.

2. Frangogiannis NG. Regulation of the inflammatory response in cardiac repair. *Circ Res*. 2012;110:159–173.

3. Kain V, Prabhu SD, Halade GV. Inflammation revisited: inflammation versus resolution of inflammation following myocardial infarction. *Basic Res Cardiol*. 2014;109:444.

4. Sugimoto MA, Sousa LP, Pinho V, Perretti M, Teixeira MM. Resolution of inflammation: what controls its onset? *Front Immunol*. 2016;7:160. https://doi.org/10.3389/fimmu.2016.00160

5. Adamo L, Rocha-Resende C, Prabhu SD, Mann DL. Reappraising the role of inflammation in heart failure. *Nat Rev Cardiol*. 2020;5:269–285.

6. Bernard D, Hansen JD, Du Pasquier L, Lefranc MP, Benmansour A, Boudinot P. Costimulatory receptors in jawed vertebrates: conserved CD28, odd CTLA4 and multiple BTLAs. *Dev Comp Immunol*. 2007;31:255–271.

7. Schildberg FA, Klein SR, Freeman GJ, Sharpe AH. Coinhibitory pathways in the B7-CD28 ligand-receptor family. *Immunity*. 2016;44:955–972.

8. Okazaki T, Tanaka Y, Nishio R, et al. Autoantibodies against cardiac troponin I are responsible for dilated cardiomyopathy in PD-1-deficient mice. *Nat Med*. 2003;9:1477–1483.

9. Nishimura H, Okazaki T, Tanaka Y, et al. Autoimmune dilated cardiomyopathy in PD-1 receptor-deficient mice. *Science*. 2001;291:319–322.

10. Murakami T, Yoshikawa T, Maekawa Y, et al. Gender differences in patients with Takotsubo cardiomyopathy: multi-center registry from Tokyo CCU Network. *PLoS One*. 2015;10:e0136655.

11. Jaworska K, Ratajczak J, Huang L, et al. Both PD-1 ligands protect the kidney from ischemia reperfusion injury. *J Immunol*. 2015;194:325–333.

12. Grasselly C, Denis M, Bourguignon A, et al. The antitumor activity of combinations of cytotoxic chemotherapy and immune checkpoint inhibitors is model-dependent. *Front Immunol*. 2018;9:2100.

13. Raedler H, Vieyra MB, Leisman S, et al. Anti-complement component C5 mAb synergizes with CTLA4Ig to inhibit alloreactive T cells and prolong cardiac allograft survival in mice. *Am J Transplant*. 2011;11:1397–1406.

14. Wei SC, Meijers WC, Axelrod ML, et al. A genetic mouse model recapitulates immune checkpoint inhibitor-associated myocarditis and supports a mechanism-based therapeutic intervention. *Cancer Discov*. 2021;11:614–625.

15. Rocha-Resende C, Weinheimer C, Bajpai G, et al. Immunomodulatory role of non-neuronal cholinergic signaling in myocardial injury. *JCI Insight*. 2019;4:e128961.

16. Weinheimer CJ, Lai L, Kelly DP, Kovacs A. Novel mouse model of left ventricular pressure

overload and infarction causing predictable ventricular remodelling and progression to heart failure. *Clin Exp Pharmacol Physiol*. 2015;42:33–40.

17. Weinheimer CJ, Kovacs A, Evans S, Matkovich SJ, Barger PM, Mann DL. Load-dependent changes in left ventricular structure and function in a pathophysiologically relevant murine model of reversible heart failure. *Circ Heart Fail*. 2018;11:e004351.

18. Schiller NB, Shah PM, Crawford M, et al. Recommendations for quantitation of the left ventricle by two-dimensional echocardiography. American Society of Echocardiography Committee on Standards, Subcommittee on Quantitation of Two-Dimensional Echocardiograms. *J Am Soc Echocardiogr*. 1989;2:358–367.

19. Lau JM, Jin X, Ren J, et al. The 14-3-3tau phosphoserine-binding protein is required for cardiomyocyte survival. *Mol Cell Biol*. 2007;27:1455–1466.

20. Rocha-Resende C, Yang W, Li W, Kreisel D, Adamo L, Mann DL. Developmental changes in myocardial B cells mirror changes in B cells associated with different organs. *JCI Insight*. 2020;5(16):e139377. https://doi.org/10.1172/jci.insight.139377

21. Adamo L, Rocha-Resende C, Lin CY, et al. Myocardial B cells are a subset of circulating lymphocytes with delayed transit through the heart. *JCI Insight*. 2020;5:e134700.

22. Butler A, Hoffman P, Smibert P, Papalexi E, Satija R. Integrating single-cell transcriptomic data across different conditions, technologies, and species. *Nat Biotechnol*. 2018;36:411–420.

23. Hafemeister C, Satija R. Normalization and variance stabilization of single-cell RNA-seq data using regularized negative binomial regression. *Genome Biol*. 2019;20:296.

24. Stuart T, Butler A, Hoffman P, et al. Comprehensive integration of single-cell data. *Cell*. 2019;177:1888–1902. e21.

25. Heng TS, Painter MW. Immunological Genome Project Consortium. The Immunological Genome Project: networks of gene expression in immune cells. *Nat Immunol*. 2008;9:1091–1094.

26. Adamo L, Staloch LJ, Rocha-Resende C, et al. Modulation of subsets of cardiac B lymphocytes improves cardiac function after acute injury. *JCI Insight*. 2018;3:e120137.

27. Zhang W, Lavine KJ, Epelman S, et al. Necrotic myocardial cells release damage-associated molecular patterns that provoke fibroblast activation in vitro and trigger myocardial inflammation and fibrosis in vivo. *J Am Heart Assoc*. 2015;4:e001993.

28. Ugolini M, Gerhard J, Burkert S, et al. Recognition of microbial viability via TLR8 drives TFH cell differentiation and vaccine responses. *Nat Immunol*. 2018;19:386–396.

29. Melmon KL, Bourne HR, Weinstein Y, Shearer GM, Kram J, Bauminger S. Hemolytic plaque formation by leukocytes in vitro. Control by vasoactive hormones. *J Clin Invest*. 1974;53:13–21.

30. Biswas S, Zimman A, Gao D, Byzova TV, Podrez EA. TLR2 plays a key role in platelet hyperreactivity and accelerated thrombosis associated with hyperlipidemia. *Circ Res*. 2017;121:951–962.

31. Onai Y, Suzuki J, Kakuta T, et al. Inhibition of IkappaB phosphorylation in cardiomyocytes attenuates myocardial ischemia/reperfusion injury. *Cardiovasc Res*. 2004;63:51–59.

32. Varricchi G, Galdiero MR, Tocchetti CG. Cardiac toxicity of immune checkpoint inhibitors: cardio-oncology meets immunology. *Circulation*. 2017;136:1989–1992.

33. Lee S, Xie J, Chen X. Peptide-based probes for targeted molecular imaging. *Biochemistry*. 2010;49:1364–1376.

34. Zouggari Y, Ait-Oufella H, Bonnin P, et al. B lymphocytes trigger monocyte mobilization and impair heart function after acute myocardial infarction. *Nat Med*. 2013;19:1273–1280.

35. Ellison GM, Torella D, Karakikes I, et al. Acute beta-adrenergic overload produces myocyte damage through calcium leakage from the ryanodine receptor 2 but spares cardiac stem cells. *J Biol Chem*. 2007;282:11397–11409.

36. Ogata A, Kimura Y, Ikenuma H, et al. Brain pharmacokinetics and biodistribution of 11C-labeled isoproterenol in rodents. *Nucl Med Biol*. 2020;86-87:52–58.

37. Shao Y, Redfors B, Ståhlman M, et al. A mouse model reveals an important role for catecholamine-induced lipotoxicity in the pathogenesis of stress-induced cardiomyopathy. *Eur J Heart Fail*. 2013;15:9–22.

38. Greenberg B, O'Connor CM, Felker GM. Classifying heart failure in the 21st century: matching taxonomy with science. *J Am Coll Cardiol HF*. 2021;9:771–773.

39. Wallner M, Duran JM, Mohsin S, et al. Acute catecholamine exposure causes reversible myocyte injury without cardiac regeneration. *Circ Res*. 2016;119:865–879.

40. Wilson HM, Cheyne L, Brown PAJ, et al. Characterization of the myocardial inflammatory response in acute stress-induced (Takotsubo) cardiomyopathy. *J Am Coll Cardiol Basic Trans Science*. 2018;3:766–778.

41. Liao X, Chang E, Tang X, et al. Cardiac macrophages regulate isoproterenol-induced Takotsubo-like cardiomyopathy. *JCI Insight*. 2022;7(3):e156236. https://doi.org/10.1172/jci.insight.156236

42. Brooks WW, Conrad CH. Isoproterenol-induced myocardial injury and diastolic dysfunction in mice: structural and functional correlates. *Comp Med*. 2009;59:339–343.

43. Sorribas M, de Gottardi A, Moghadamrad S, et al. Isoproterenol disrupts intestinal barriers activating gut-liver-axis: effects on intestinal mucus and vascular barrier as entry sites. *Digestion*. 2020;101:717–729.

44. Beswick EJ, Johnson JR, Saada JI, et al. TLR4 activation enhances the PD-L1–mediated tolerogenic capacity of colonic CD90^{+} stromal cells. *J Immunol*. 2014;193:2218–2229.

45. Liu X, Hogg GD, DeNardo DG. Rethinking immune checkpoint blockade: 'Beyond the T cell. *J Immunother Cancer*. 2021;9:e001460.

46. Seko Y, Yagita H, Okumura K, Azuma M, Nagai R. Roles of programmed death-1 (PD-1)/PD-1 ligands pathway in the development of murine acute myocarditis caused by coxsackievirus B3. *Cardiovasc Res*. 2007;75:158–167.

47. Baban B, Liu JY, Qin X, Weintraub NL, Mozaffari MS. Upregulation of programmed death-1 and its ligand in cardiac injury models: interaction with GADD153. *PLoS One*. 2015;10:e0124059.

48. Chaudhri A, Xiao Y, Klee AN, Wang X, Zhu B, Freeman GJ. PD-L1 Binds to B7-1 Only In Cis on the Same Cell Surface. *Cancer Immunol Res*. 2018;6:921–929.

49. Zhao Y, Lee CK, Lin C-H, et al. PD-L1:CD80 Cis-heterodimer triggers the co-stimulatory receptor CD28 while repressing the inhibitory PD-1 and CTLA-4 pathways. *Immunity*. 2019;51:1059–1073.e9.

50. Ederhy S, Dolladille C, Thuny F, Alexandre J, Cohen A. Takotsubo syndrome in patients with cancer treated with immune checkpoint inhibitors: a new adverse cardiac complication. *Eur J Heart Fail*. 2019;21:945–947.

51. Baik AH, Oluwole OO, Johnson DB, et al. Mechanisms of cardiovascular toxicities associated with immunotherapies. *Circ Res*. 2021;128:1780–1801.

52. Kim JE, Patel K, Jackson CM. The potential for immune checkpoint modulators in cerebrovascular injury and inflammation. *Expert Opin Ther Targets*. 2021;25:101–113.

53. Qin W, Hu L, Zhang X, et al. The diverse function of PD-1/PD-L pathway beyond cancer. *Front Immunol*. 2019;10:2298. https://doi.org/10.3389/fimmu.2019.02298

KEY WORDS **inflammation, myocardial homeostasis, PD-1, PD-L1, tissue injury**

APPENDIX **For supplemental tables and figures as well as a supplemental file containing the list of differentially expressed genes in the LYVE1- macrophages on day 2 relative to baseline levels, please see the online version of this paper.**